# SPECTROSCOPY OF METAL ATOMS AND METALLIC OXIDES IN RARE GAS MATRICES

By

WARREN DEWEY HEWETT, JR.

A DISSERTATION PRESENTED TO THE GRADUATE COUNCIL OF
THE UNIVERSITY OF FLORIDA
IN PARTIAL FULFILLMENT OF THE REQUIREMENTS FOR THE
DEGREE OF DOCTOR OF PHILOSOPHY

UNIVERSITY OF FLORIDA

1974

TABLE OF CONTENTS

Page

LIST OF TABLES

LIST OF FIGURES

ABSTRACT

INTRODUCTION. . . . . 1

REFERENCES, INTRODUCTION. . . . . 6

Chapters

I OPTICAL SPECTROSCOPY OF BERYLLIUM ATOMS IN RARE GAS MATRICES. . . . . 7

Introduction. . . . . 7
Experimental. . . . . 9
Observations. . . . . 13
Discussion. . . . . 36
Summary . . . . . 51

REFERENCES, CHAPTER I . . . . . 53

II OPTICAL SPECTROSCOPY OF BERYLLIUM DIMERS IN RARE GAS MATRICES. . . . . 56

Introduction. . . . . 56
Experiments and Observations. . . . . 58
Assignment of $Be_2$ Bands . . . . . 67
Discussion. . . . . 70
Summary . . . . . 79

REFERENCES, CHAPTER II. . . . . 81

III SPECTROSCOPY OF MOLYBDENUM AND MOLYBDENUM OXIDES IN RARE GAS MATRICES . . . . . 83

Introduction. . . . . 83
Experimental. . . . . 88
Observations. . . . . 93

Page

Discussion. . . . . .138

REFERENCES, CHAPTER III . . . . . .144

BIOGRAPHICAL SKETCH. . . . . .147

## LIST OF TABLES


| Table | | Page |
|---|---|---|
| 1 | ABSORPTION LINES IN Be·RARE GAS SYSTEMS | 14 |
| 2 | ABSORPTION BANDS OF $A^1\Sigma_u^+ \leftarrow X^1\Sigma_g^+$ of $Be_2$ IN A NEON MATRIX AT 4°K | 62 |
| 3 | ABSORPTION BANDS OF $A^1\Sigma_u^+ \leftarrow X^1\Sigma_g^+$ OF $Be_2$ IN AN ARGON MATRIX AT 4°K | 63 |
| 4 | $C_{AB} \cdot 10^{60}$, erg · cm$^6$ | 66 |
| 5 | $A^1\Sigma_u^+ \leftarrow X^1\Sigma_g^+$ TRANSITIONS OF GROUP IIA DIMER MOLECULES AND VIBRATIONAL FORCE CONSTANTS | 78 |
| 6 | PHYSICAL PROPERTIES OF THE REFRACTORY METALS AND THEIR OXIDES | 84 |
| 7 | ULTRAVIOLET AND VISIBLE SPECTRA IN ARGON MATRICES | 94 |
| 8 | ULTRAVIOLET ABSORPTIONS IN NEON MATRICES | 105 |
| 9 | ABSORPTIONS OF Mo POLYMERS IN NEON MATRICES | 109 |
| 10 | MAJOR INFRARED ABSORPTIONS OBSERVED FOR THE SPECIES VAPORIZED FROM HOT $MoO_3$(s) AND TRAPPED IN ARGON MATRICES | 114 |
| 11 | MAJOR INFRARED ABSORPTIONS OBSERVED FOR THE SPECIES VAPORIZED FROM HOT $MoO_3$(s) AND TRAPPED IN NEON MATRICES | 115 |
| 12 | NATURAL OCCURRING STABLE ISOTOPES OF Mo | 122 |
| 13 | ISOTOPIC FREQUENCIES FOR Mo OXIDES IN Ne MATRICES | 129 |
| 14 | VIBRATIONAL FREQUENCIES OF MOLYBDENUM OXIDE MOLECULES FROM INFRARED SPECTRA OF NEON MATRICES | 141 |
| 15 | COMPARISON OF W AND Mo OXIDES IN NEON MATRICES AT 4°K | 142 |

LIST OF FIGURES


| Figure | | Page |
|---|---|---|
| 1. | Matrix isolation technique as applied to molecules vaporizing at a high temperature. | 4 |
| 2. | Gas phase atomic energy level diagram for beryllium. The wavelengths of the indicated transitions are given in nm. | 16 |
| 3. | Beryllium resonance absorption in an argon matrix. | 18 |
| 4. | Absorption spectrum of beryllium atoms in an argon matrix, showing features assigned as "pumping bands." | 19 |
| 5. | 214.7 nm absorption in a Be doped Ar matrix at 4°K. | 20 |
| 6. | Spectrum indicating the formation of $Be_2$ molecules in an Ar matrix. | 22 |
| 7. | Be polymer absorption in a highly concentrated Ar matrix | 23 |
| 8. | Ultraviolet absorption spectra of Be atoms in Ne matrices at 4°K. | 25 |
| 9. | Impurity absorptions observed in a Be doped Na matrix at 4°K. | 26 |
| 10. | Ultraviolet absorption spectra of Be atoms in Kr matrices. | 28 |
| 11. | Spectrum of the long-lived emission observed in a Be doped Ar matrix. | 30 |
| 12. | Emission spectrum of Be isolated in a Kr matrix. | 31 |
| 13. | Decay curve for the 465 nm emission in Ar matrices. | 33 |
| 14. | Plot of ln(Emission Intensity) vs. Time for the decay of the 465 nm emission in Kr matrices. | 34 |

| Figure | | Page |
|---|---|---|
| 15. | Plot of ln(Emission Intensity) vs. Time for the decay of the 517 nm emission in Kr matrices. | 35 |
| 16. | Calculated relative intensities of the quantum mechanical delta functions and the semiclassical line shapes for the multi-phonon band envelopes. | 48 |
| 17. | Ultraviolet absorption spectrum of $Be_2$ in an Ne matrix. | 59 |
| 18. | Ultraviolet absorption spectrum of $Be_2$ in an Ar matrix. | 60 |
| 19. | A schematic diagram of the potential energy curves for low lying states of the $Be_2$ molecule. | 72 |
| 20. | Birge-Sponer plot for $Be_2$ in Ar. | 75 |
| 21. | Apparatus for the production of Mo oxides. | 90 |
| 22. | Ultraviolet absorption spectra of Mo atoms and Mo oxides in Ar matrices. | 97 |
| 23. | Near infrared absorption spectrum of species vaporized from hot $MoO_3$(s) and trapped in an Ar matrix. | 98 |
| 24. | Ultraviolet spectrum of a Ne matrix containing Mo atoms and Mo oxides. | 100 |
| 25. | $e^7P \leftarrow e^7S$ absorption of Mo atoms in a Ne matrix. | 101 |
| 26. | Far ultraviolet absorption spectrum of a Ne matrix containing Mo oxides. The absorption peaks are at 212.0, 229.5, and 243 nm. | 103 |
| 27. | Far ultraviolet absorption spectrum of a Ne matrix containing Mo oxides--expanded scale. | 104 |
| 28. | Mo polymer absorption (possible $Mo_2$) in a Ne matrix. | 106 |
| 29. | Mo polymer absorption in a Ne matrix. | 107 |
| 30. | Infrared absorption spectrum of an Ar matrix containing species vaporized from hot $MoO_3$(s). | 112 |
| 31. | Infrared absorption spectrum of a Ne matrix containing species vaporized from hot $MoO_3$(s). | 113 |

Figure Page

32. Ring structure of the metal oxide molecules $(MO_3)_3$, where M is Molybdenum or Tungsten. 117

33. Infrared absorption spectrum of a Ne matrix containing Mo oxides formed by passing $O_2$ gas through a Mo cell at 1725°C. 120

34. Infrared absorption spectrum of an Ar matrix containing Mo oxides formed by passing $O_2$ gas through a Mo cell at 1725°C. 121

35. Infrared absorption spectrum of an Ar matrix containing Mo oxide formed by passing $O_2$ gas through a Mo cell at 2100°C. 126

36. Infrared absorption spectrum of a Ne matrix containing Mo oxides formed by passing $O_2$ gas through a Mo cell at 2100°C. 117

37. High resolution infrared absorption spectrum of a Ne matrix containing Mo oxides formed at high temperatures (2100°C) using $^{16}O_2$. 128

38. High resolution infrared absorption spectrum of a Ne matrix containing Mo oxides formed at high temperatures (21°C) using $^{18}O_2$. 133

39. Infrared absorption seen after $H_2$ photolysis of a 0.1% $O_2$ in Ne matrix containing Mo atoms. 136

40. High resolution scan of the 1040 $cm^{-1}$ band shown in Figure 39. 137

Abstract of Dissertation Presented to the Graduate Council of the University of Florida in Partial Fulfillment of the Requirements for the Degree of Doctor of Philosophy

# SPECTROSCOPY OF METAL ATOMS AND METALLIC OXIDES IN RARE GAS MATRICES

By

Warren Dewey Hewett, Jr.

August, 1974

Chairman: Professor William Weltner, Jr.
Major Department: Chemistry

Be atoms, Mo atoms, and Mo oxides have been trapped in solid rare gas matrices at 4°K and investigated by ultraviolet, visible, and infrared spectroscopy. The atomic species were produced as molecular beams by vaporizing the metals. Beams of Mo oxides were produced by passing $O_2$ gas over hot Mo metal or, alternatively, by vaporizing $MoO_3$(s) from a resistively heated Ta cell. The species observed were Be atoms, $Be_2$, Mo atoms, $MoO_2$, $MoO_3$, $(MoO_3)_2$, and $(MoO_3)_3$.

Be atoms, trapped in solid Ne, Ar and Kr, showed a strong absorption near 235 nm which was assigned to the resonance transition $^1P_1 \leftarrow {}^1S_0$ which appears at 234.86 nm (42,565 $cm^{-1}$) in the gas phase. Specifically, the absorption occurred at 232.0 nm (43,090 $cm^{-1}$), 236.0 nm (42,360 $cm^{-1}$), and 240.5 nm (41,567 $cm^{-1}$) in Ne, Ar, and Kr, respectively. Excitation to the $^1P$ state also led to long-lived emission in Ar and Kr matrices at 465.0 nm and 464.7 nm with lifetimes of 1.33(8) and 0.095(5) sec, respectively. The emission was assigned to

the spin-forbidden $^3P \rightarrow {}^1S$ emission. In each case a broad band also appeared in emission at longer wavelengths and was attributed to coupling with the matrix phonons.

A progression of absorption bands assignable to $Be_2$ was observed with the (0,0) band at 350.15(5) nm (28,551 $cm^{-1}$) in Ne and 361.30(5) nm (27,670 $cm^{-1}$) in Ar. In analogy with the other van der Waals molecules $Mg_2$ and $Ca_2$, these bands were assigned to the $A^1\Sigma_u^+ \rightarrow X^1\Sigma_g^+$ transition. The vibrational frequency in the upper state was 489 $cm^{-1}$ in Ne and 474 $cm^{-1}$ in Ar matrices. No other electronic transitions assignable to $Be_2$ were detected out to 50,000 $cm^{-1}$.

Mo atoms trapped in solid Ne and Ar showed strong absorptions in the ultraviolet region which were assigned to transitions from the ground state, $a\,{}^7S_3$, to the excited states $y^7P_{2,3,4}$ and $z^7P_{2,3,4}$. In Ar the $z^7P \rightarrow a^7S$ transition appeared as a triplet with peaks at 357.1, 349.9, and 341.5 nm. The $y^7P \rightarrow a^7S$ transition appeared as a single broad band at 288.0 nm. In Ne matrices the $z^7P \rightarrow a^7S$ triplet was seen at 371.5, 366.5, and 359.2 nm. The $y^7P \rightarrow a^7S$ transition also appeared as a triplet in solid Ne, with peaks at 307.4, 305.5, and 303.0 nm. Bands assigned to Mo polymers were observed near 510 nm in concentrated Ne matrices, and a progression tentatively assigned to $Mo_2$ was observed in Ne from about 345 nm to 320 nm with a vibrational spacing in the excited state of about 550 $cm^{-1}$.

$MoO_2$, $MoO_3$, $(MoO_3)_2$, $(MoO_3)_3$, $(MoO_3)_4$, and $(MoO_3)_5$ have been trapped in Ne and Ar matrices at 4°K. The electronic absorptions of these molecules were extremely weak and not at

all similar to the tungsten oxide systems. The infrared spectra were recorded and the bands were assigned to particular molecules on the basis of the relative abundances of the oxides under different reaction conditions, as determined by previous mass spectrometric investigations. Bands assignable to $\nu_3$ and $\nu_1$ for $^{98}Mo^{16}O_2$ were observed in Ne at 900.1 $cm^{-1}$ and 949.5 $cm^{-1}$, respectively. Isotopic substitution with $^{18}O_2$ allowed the O-Mo-O bond angle to be calculated, and it was determined to be 124° ± 6°. Absorptions at 975.7 $cm^{-1}$ and 922.2 $cm^{-1}$ in Ne were assigned to $MoO_3$. Bands at 975.7, 694.2, and 350.1 $cm^{-1}$ were assigned to $(MoO_3)_2$ in Ne, and absorptions at 977.6, 858.4, and 840.1 $cm^{-1}$ were assigned to the trimer, $(MoO_3)_3$, in Ne matrices.

## INTRODUCTION

The characterization of chemical reactions which occur in the gas phase at high temperatures and chemical species which are formed under these conditions has held the interest of the scientific world since the inception of the experimental age. Certainly most of the earliest work was concerned with reactions in hydrocarbon flames and with reactions which could be carried out at the temperatures available in air-hydrocarbon flames. In recent decades the constantly increasing temperature range available to the experimentalist and the multiplicity of methods of generating high temperatures have broadened the scope of high temperature chemistry to include materials research, thermodynamics, kinetics, molecular structure determination, and the study of reactive intermediates, among others.

Historically the basic investigative techniques of the high temperature scientist have been thermometry and spectroscopy, the former being necessary to define the temperature domain of interest and the latter in its various forms to reveal the composition and structures of the systems under study. Although the advances in temperature measurement have been many and important, the overwhelming impetus given to the study of high temperature systems has come from the improvements in molecular and atomic spectroscopy and the

marriage of new experimental techniques, namely mass spectrometry, with the conventional methods of spectroscopic analysis.

This combination of techniques enables the spectroscopist to analyze his data with prior knowledge as to the nature of the species which are actually present and their relative abundances at a given temperature and pressure. With this information to help sort his data, the spectroscopist can more easily determine energy levels, thermodynamic parameters, bond lengths, bond angles and other structural data for the species in the system.

There remain many experimental difficulties in identifying and characterizing high temperature species. The compounds produced tend to be extremely reactive and hence have short lifetimes during which they may be examined. This necessitates working at low pressure in flowing systems which in turn give weak absorption spectra requiring long optical paths. Aside from the many other experimental difficulties in studying reactive gases at high temperatures, there is also the physical difficulty, that a system in equilibrium with its surroundings will achieve a Boltzmann distribution of its members among the various energy levels which are available to them within the range of a few kT. This complicates the task of assigning observed spectral lines to specific energy levels and makes the ordering of the observed electronic states a difficult job.

To overcome the difficulties mentioned above, the technique of matrix isolation spectroscopy was proposed independantly

by Norman and Porter [1] and by Whittle, Dows, and Pimentel [2] in 1954. The basic idea behind the technique is that if the reactive species of interest can be immobilized in an inert medium or matrix, any further reaction is minimized, and the specimen is preserved for conventional spectroscopic analysis. Furthermore, since the trapped species are at temperatures which are usually below 25°K, only their ground electronic and vibrational states are significantly occupied, which simplifies the observed spectra immensely. This idea was developed into a workable technique by Pimentel [3] at Berkeley using rigid matrices of nitrogen and argon, and has now been extended to almost every conceivable type of matrix material and a tremendous variety of solutes.

In the years since the discovery of matrix isolation spectroscopy there have been many variations on the theme, but a general technique has been developed which is followed fairly closely in every case. Schematically the process is shown in Figure 1. The species of interest are produced under high vacuum in a source (high temperature cell, RF discharge, electric discharge, etc.) and are collimated into a crude molecular beam which impinges on the trapping surface, typically a material transparent to radiation in the spectral region of interest, which has been cooled to 4°K or 20°K by a reservoir of liquid helium or liquid hydrogen in thermal contact with it. At the same time, the matrix material (usually one of the rare gases) is sprayed onto the trapping surface in quantities such that M/R (the ratio of

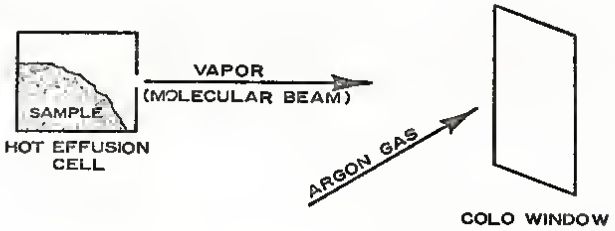


Figure 1. Matrix isolation technique as applied to molecules vaporizing at a high temperature.

the number of moles of matrix material to the number of moles of trapped species) is 500:1 or greater. After the matrix has been made the trapped material is available for spectroscopic analysis until the refrigerant fluid is exhausted and the matrix evaporates. A recent review of this experimental technique and the work accomplished with it is contained along with an extensive bibliography in the book by Meyer [4].

The work presented here includes the application of matrix isolation spectroscopy to one system which is chemically simplistic and another which is considerably more complex. The first study deals with the matrix isolated products formed when pure beryllium metal is vaporized under vacuum and leads to discussions of atomic spectra in matrices and van der Waals molecules. The second part of this work deals with the species formed when molybdenum reacts with oxygen gas under a variety of experimental conditions with the reaction products trapped and analyzed spectroscopically.

## REFERENCES, INTRODUCTION


1. I. Norman and G. Porter, Nature 174, 508 (1954).

2. E. Whittle, D.A. Dows, and G.C. Pimentel, J. Chem. Phys. 22, 1943 (1954).

3. E.D. Becker and G.C. Pimentel, J. Chem. Phys. 25, 224 (1956).

4. B. Meyer, Low Temperature Spectroscopy (American Elsevier, New York, 1971).

CHAPTER I

# OPTICAL SPECTROSCOPY OF BERYLLIUM ATOMS IN RARE GAS MATRICES

## Introduction

When metal atoms are trapped in rare gas matrices, the gas phase resonance transitions are usually identifiable in the solid, but the absorption spectrum is commonly altered in several ways [1]. The energies of the observed transitions are nearly always different from the gas phase values, and transitions which are seen as sharp singlets in the gas phase may appear as broad multiplets in the matrix. New absorptions are often recorded which have no obvious correlation with previously observed atomic transitions, and forbidden transitions may become allowed because of relaxed selection rules in the rare gas solids. The observation of these complexities in the electronic spectra of matrix isolated atoms has stimulated the experimental and theoretical effort directed toward the classification and explenation of these phenomena.

A great deal of the work which has been done on atomic species in matrices has dealt with the np ← ns resonence transitions of metals having singly or doubly occupied ns shells as the outermost populated orbitals in their ground electronic states (alkali metals [2-7], alkaline earths [8-14], Group

IIb metals [2,15-21], and transition metals [8,17,22-25]). Commonly, the resonance transition appears in the matrix as a triplet for atoms of these configurations. Attempts to explain the triplet splitting have been related to several different theoretical models: (1) Jahn-Teller distortion of the $^1P_1$ state, removing its threefold degeneracy [17], (2) solute-solute interactions between non-nearest neighbor metal atoms [2], (3) non-octahedral symmetry of the trapping site [3,9], which could split the degeneracy of the excited state, and (4) multiple trapping sites of different energies [7,17]. Recent experiments [23] have indicated that the observed complexity of the absorption spectra of metal atoms in solid matrices is not due to solute-solute interactions, and the observed behavior of the triplet systems when the matrices are annealed [12] indicates that multiple trapping sites are not the origin of the energy splitting. However, there is still no single theoretical model which satisfactorily describes the phenomena which are observed for these systems.

The beryllium atom is particularly interesting for matrix study because of its small size and relatively simple electronic properties. The ground state electron configuration is $1s^2 2s^2$, and the atomic resonance transition $2s2p\ ^1P_1 \leftarrow 2s^2\ ^1S_0$ is the primary absorption in the matrix and in the gas phase where it occurs at 234.86 nm (42 565 $cm^{-1}$) [26]. The low lying energy levels of the Be atom are shown in Figure 2. Although the singlet and triplet manifolds of the Be atomic

system have been thoroughly investigated [27-31], the intersystem combinations which are spin forbidden have been rarely seen [32] and not definitely assigned. This is as expected since for a light atomic species in the gas phase, the selection rule $\Delta S = 0$ should be rigorously true. In the matrix, however, the perturbation introduced by the cage of rare gas atoms surrounding the Be atom may cause the $\Delta S = 0$ rule to be relaxed, and in fact, a transition has been observed in emission which is relatively long lived and has been assigned to a $^3P \rightarrow {}^1S$ intersystem combination.

## Experimental

The dewars used in this work are similar to those described earlier [33,34]. The matrices were formed on calcium fluoride or sapphire targets cooled with liquid helium so that the temperature of the trapping surface was about 4°K. In the variable temperature experiments, the temperature of the trapping surface was measured with a chromel-Au(0.07% Fe) thermocouple attached to the copper block on which the trapping target was mounted. The thermocouple voltage was monitored using a Leeds and Northrup model 8687 volt potentiometer. The dewar vacuum system was independent of the furnace to allow true differential pumping, and the background pressure in the dewar was typically $2 \times 10^{-7}$ torr before filling with liquid helium and $4 \times 10^{-8}$ torr after filling.

The furnace has been described previously [33] and was equipped with demountable flanges to permit the use of cells

heated inductively or resistively. The furnace chamber was routinely evacuated to a pressure of $2 \times 10^{-7}$ torr before an experiment was begun. The beryllium was vaporized from resistively heated tungsten cells which had previously been outgassed under high vacuum at about 2000°C. The sample deposition temperature was determined by measurement of the surface temperature of the tungsten cell with a calibrated Leeds and Northrup optical pyrometer. The cell temperatures which are reported here have been corrected for the known emissivity of tungsten surfaces using the data of Jones [35] as recorded in the book by Epps [36].

The rare gases argon and krypton were Matheson research grade. Ultra-pure neon was purchased from Airco. Beryllium metal was purchased from Electronic Space Products, Inc., with a stated purity of 99.99%. With the exception of passing the neon and argon through a liquid nitrogen trap before deposition, all of these materials were used without further purification.

Realizing the possible health hazard [37,38] of beryllium and its oxides, special safety precautions were taken to avoid direct handling of these materials. When the dewar or furnace was opened after a series of experiments, all parts which might have been contaminated with the beryllium vapor were cleaned in dilute sulfuric acid solution. During these operations the work area was covered with absorbent paper, and the investigators wore dust masks and disposable lab coats and gloves.

A series of experiments was run in neon, argon, and krypton matrices to determine the effects of different host materials on the spectroscopic properties of the trapped beryllium. During these experiments the rare gases were deposited at rates of 6 liter-torr/min. The beryllium concentration in the matrix was varied by changing the temperature of the tungsten effusion cell over the range 1100-1400°C which corresponds to beryllium vapor pressures of $10^{-3}$ torr to $10^{-1}$ torr. Typical experiments involved deposits of 10-20 minutes followed by spectroscopic examination of the resulting matrix and further deposits and spectral scans as needed.

Absorption spectra were recorded from 685 to 199 nm using a Jarrell Ash 0.5 meter Ebert mount monochromator. Gratings ruled with 1200 lines/mm and blazed at 500 and 300 nm were used to span this spectral range, and with these gratings the instrument had a reciprocal linear dispersion of 1.6 nm/mm in the first order. The detectors were RCA 7200 and RCA 1P21 photomultiplier tubes. The photomultiplier output was processed by a Jarrell Ash 82110 recording electronic system and displayed on a Bristol model 570, 0-10 mv strip chart recorder. In the visible region a tungsten ribbon-filament lamp was used as the spectral source, and a Sylvania, DE350 deuterium lamp was used in the ultraviolet. Before beryllium deposits were made, background absorption spectra of the trapping target covered with a thin film of the rare gas in use were recorded. All of the spectra were calibrated using a

low pressure mercury arc lamp, and wavelengths were measured to the nearest 0.5 nm unless otherwise noted. Emission spectra were excited using the deuterium lamp and an Oriel Optics Corporation F-11-20 monochromator as a source of narrow bandwidth, far ultraviolet radiation. With the monochromator set at 235 nm, the excitation bandwidth was 8.0 nm fwhm (full width at half maximum intensity). A Pyrex lens was used to focus the matrix emission on the entrance slits of the Jarrell Ash monochromator mentioned above. The lens also acted as an ultraviolet filter, keeping the exciting light from reaching the detector as the second order spectrum from the diffraction grating.

To measure the lifetime of the emission, the exciting light was mechanically chopped, and the output of the photomultiplier was displayed on a Hewlett-Packard 180A oscilloscope with the 1801Q dual channel vertical amplifier and the 1820A timebase. The oscilloscope trace was photographed and the decay curve was measured from the photograph. An alternative method of recording the decay curve, as well as the growth curve, which was also examined, was to take the amplified photomultiplier signal from the Jarrell Ash electrometer output and record it on a Moseley 2D-2 XY recorder with internal timebase. This method gave results which were consistent with those obtained from the oscilloscope display and had the advantage of giving the data in a more easily measurable form.

## Observations

The results of the experiments in the different matrix materials are presented in the following sections. A list of the main absorption peaks which were observed and their relative intensities can be found in Table 1.

### Beryllium Absorption in Argon

The absorption spectrum of beryllium in argon was the most complex of the systems studied. When Be was deposited slowly at temperatures below 1150°C, the atomic resonance transition was observed as a strong triplet (Figure 3) with peaks at 237.0, 236.0, and 235.0 nm, having a full width at half maximum (fwhm) of 620 $cm^{-1}$ for the total triplet system. As the concentration of Be in the matrix was increased, the resonance transition became almost totally absorbing with a linewidth of about 1500 $cm^{-1}$ fwhm, and the triplet structure was no longer observed. One argon matrix was prepared which had an intermediate concentration of Be atoms and showed no absorption above 250 nm. When first scanned, the atomic resonance line was structureless and nearly totally absorbing with a well-defined sideband at 243.6 nm which was approximately 20 percent as intense as the resonance line. As the spectrum was repeatedly scanned, the sideband slowly disappeared and the previously mentioned triplet structure developed in the resonance line, indicating that an annealing process was taking place in the matrix. When the optical density of the

TABLE 1

ABSORPTION LINES IN Be:RARE GAS SYSTEMS

| Wavelength nm | Wavenumber $cm^{-1}$ | Intensity* Dilute | Concentrated | Assignment |
|---|---|---|---|---|
| | | Be:Neon | | |
| 232.0 | 43 090 | s | vs | $2s2p\ ^1P \leftarrow 2s^2\ ^1S$ |
| 242.4 | 41 241 | w | m | $2s2p\ ^1P \leftarrow 2s^2\ ^1S$ |
| 258.0 | 38 748 | --- | w | unknown |
| 246.4 | 40 572 | --- | w | impurity |
| 252.2 | 39 639 | --- | w | impurity |
| 258.2 | 38 718 | --- | w | impurity |
| "$Be_2$ Bands" | | (see Table 2) | | |
| | | Be:Argon | | |
| 216.2 | 46 239 | w | m | $2s4d\ ^3D \leftarrow 2s2p\ ^3P$ |
| 217.2 | 46 026 | w | m | $2s4d\ ^3D \leftarrow 2s2p\ ^3P$ |
| 235.0 | 42 540 | s | vs | $2s2p\ ^1P \leftarrow 2s^2\ ^1S$ |
| 236.0 | 42 360 | s | vs | $2s2p\ ^1P \leftarrow 2s^2\ ^1S$ |
| 237.0 | 42 181 | s | vs | $2s2p\ ^1P \leftarrow 2s^2\ ^1S$ |
| 262.6 | 38 069 | vw | w | $2p^2\ ^3P \leftarrow 2s2p\ ^3P$ |
| 270.8 | 36 916 | vw | w | $2p^2\ ^3P \leftarrow 2s2p\ ^3P$ |
| 287.0 | 34 833 | --- | m | Be polymers |
| 289.0 | 34 591 | --- | m | Be polymers |
| 291.6 | 34 282 | --- | s | Be polymers |
| "$Be_2$ Bands" | | (see Table 3) | | |

TABLE 1 (continued)

| Wavelength nm | Wavenumber $cm^{-1}$ | Intensity* | | Assignment |
|---|---|---|---|---|
| | | Dilute | Concentrated | |
| | | Be:Krypton | | |
| 240.5 | 41 567 | s | s | $2s2p\ ^1P \leftarrow 2s^2\ ^1S$ |
| 359.0 | 27 847 | --- | w | $Be_2$ |
| 365.5 | 27 352 | --- | w | |
| 372.2 | 26 859 | --- | w | |

*w, m and s = weak, medium, and strong, respectively. vw = very weak, etc.

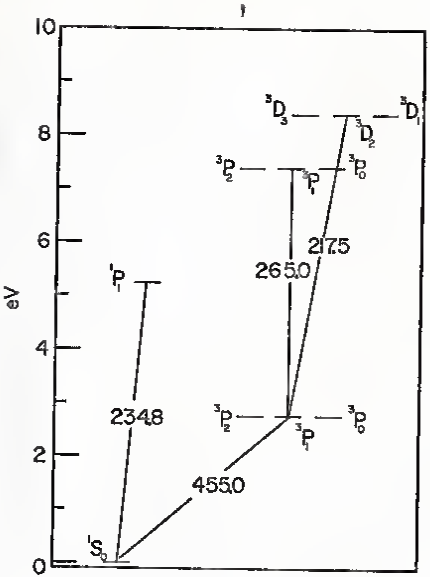


Figure 2. Gas phase atomic energy level diagram for beryllium. The wavelengths of the indicated transitions are given in nm.

matrix was further increased, absorption bands appeared at 270.8, 262.6 (Figure 3), and 261.7 nm (Figure 4), and when the Be concentration was further increased a band system was observed from 362.0 to 328.9 nm which is attributed to the $Be_2$ molecule (see below).

A long-lived blue green emission of light was observed from all of the Be doped argon matrices which were prepared in these experiments (see below for further discussion). Once it had been ascertained that the emitted light was coming from an excited beryllium moiety, probably the lowest triplet level of the atom, the possibility arose that some of the weaker absorptions seen in the matrix might have been "pumping bands," absorptions from the metastable $2s2p\ ^3P$ atomic state to higher triplet states.

In order to test this hypothesis, a series of scans was made from 280 nm to 245 nm using a Corning 7-54 filter to attenuate short wavelength ultraviolet radiation. The filter was first placed between the light source and the sample and then it was moved to a position between the sample and monochromator slits. It was found that the absorptions at 270.8 and 262.6 nm were only observed when the sample received unfiltered radiation from the $D_2$ lamp. Unfortunately we were not equipped to do a similar test on the 216.7 nm absorption.

An analogous procedure was used to verify that the bands assigned to $Be_2$ were not dependent on atomic excitation. A Pyrex lens was placed first between sample and source and

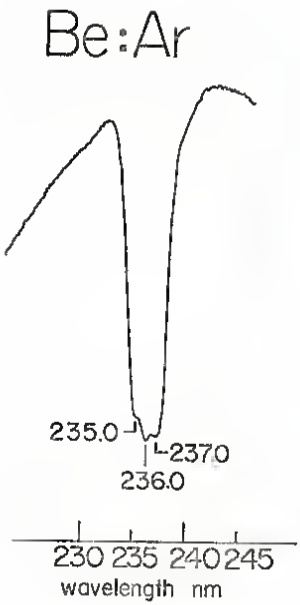


Figure 3. Beryllium resonance absorption in an argon matrix.

Figure 4. Absorption spectrum of beryllium atoms in an argon matrix, showing features assigned as "pumping bands."

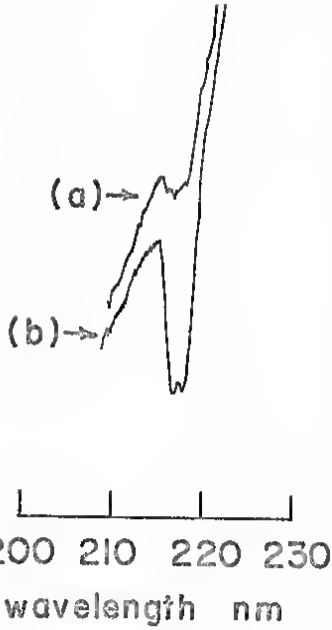


Figure 5. 216.7 nm absorption in a Pb doped Ar matrix at 4°K. (a) Before annealing. (b) After annealing.

then between sample and monochromator. No change was observed in the $Be_2$ band intensities under these conditions, indicating that the "$Be_2$ bands" were not assignable as atomic or molecular pumping bands.

A variable temperature experiment was done to investigate the diffusion of Be atoms in the argon matrix. A matrix was deposited at 4°K which showed absorptions at 270.8, 262.6, and 216.7 nm along with the $Be_2$ bands and the atomic resonance absorption which had a strong shoulder on the red side. The matrix was warmed to about 25°K, and another absorption spectrum was measured. The $Be_2$ bands were increased in intensity (see Figure 6), the 270.8 and 262.6 nm absorptions were considerably weakened, the resonance absorption line was weakened and sharpened, the red shoulder on the resonance line was decreased in intensity, the 216.7 nm band began to show doublet structure, and a new band appeared at 291.6 nm. As the matrix was warmed further, the band at 216.7 nm was annealed to a clearly resolved doublet with peaks at 216.2 and 217.2 nm as shown in Figure 4, and the $Be_2$ bands continued to grow in intensity.

The absorption band at 291.6 nm was also observed in several highly concentrated argon matrices along with weaker absorptions at 289.0 and 287.0 nm (see Figure 7). These bands are assigned to Be polymers such as $Be_3$ or $Be_4$ because they grow in when the matrices are annealed, and their intensities vary with respect to the $Be_2$ band intensities, indicating that they belong to different species.

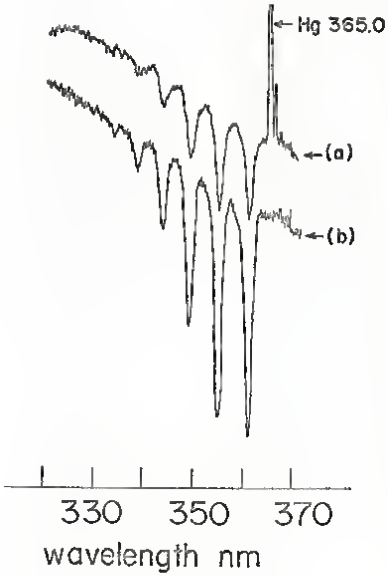


Figure 6. Spectrum indicating the formation of $Be_2$ molecules in an Ar matrix. (a) Spectrum recorded after initial deposit. (b) Spectrum recorded after the matrix was annealed.

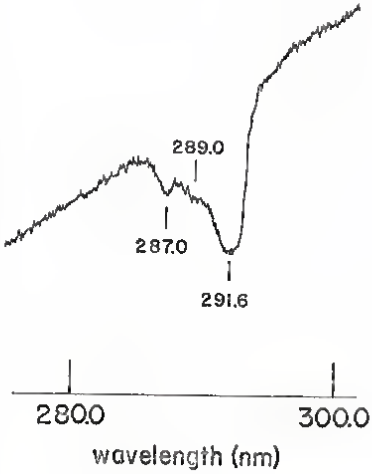


Figure 7. Be polymer absorption in a highly concentrated Ar matrix.

Beryllium Absorption in Neon

The spectra of beryllium in neon matrices were recorded over a range of different matrix concentrations by depositing the metal at different rates as was done in argon matrices. It can be seen in Figure 8, however, that even in the most dilute matrices the Be atom resonance transition was always a broad (1350 $cm^{-1}$ fwhm) absorption showing no fine structure. The resonance line, which was blue shifted from the gas phase transition energy by about 500 $cm^{-1}$, was seen at 232.0 nm and was the most intense absorption seen prior to annealing. Absorptions were also recorded at 242.4 and 258.0 nm along with the $Be_2$ bands which are discussed in a separate section. The absorption at 242.4 nm (see Figure 9) was always weaker than the resonance line and decreased in intensity as the matrix was annealed. The 258.0 nm absorption was weak and very broad (2300 $cm^{-1}$ fwhm). When the matrix was strongly annealed, the Be atomic absorption disappeared as the $Be_2$ bands grew in intensity.

In one of the most concentrated neon matrices, bands were recorded at 246.4, 252.2, and 258.2 nm (see Figure 9). These absorptions were weak but well defined, and were probably due to an impurity since they do not appear in any of the other experiments.

Beryllium Absorption in Krypton

The krypton matrices showed the fewest absorption bands

Figure 8. Ultraviolet absorption spectra of Be atoms in Ne matrices at 4°K. The upper spectrum was observed for an extremely dilute matrix. The lower spectrum was recorded in a matrix having a higher Be concentration.

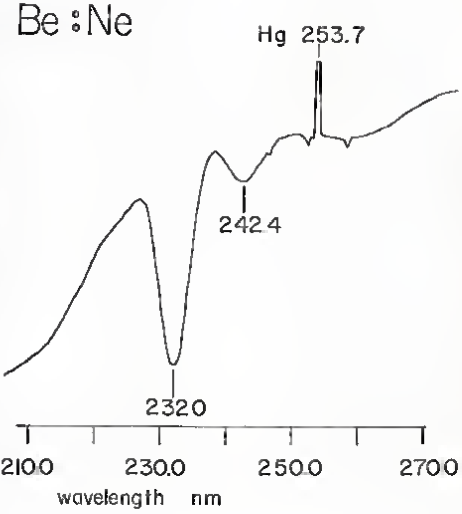


Figure 9. Impurity absorptions observed in a Be doped Ne matrix at 4°K. The broad band at 242.4 nm disappeared when the matrix was annealed.

among the rare gases used in this work. At low and high concentrations the only absorption detected was at 240.5 nm (see Figure 10). This was attributed to the $^1P \leftarrow {}^1S$ atomic resonance transition and was found to be red shifted by 1000 $cm^{-1}$ from the gas phase transition energy. The absorption appeared to have some unresolved structure at low concentrations (see Figure 10) which was unseen in more concentrated matrices. Only at deposition temperatures above 1380°C were any bands seen in the region where the $Be_2$ bands were observed in neon and argon matrices. The observed absorptions are listed in Table 1. They were very weak and not readily identifiable as a vibrational progression even in highly concentrated matrices.

Emission Spectra and Lifetimes

Emission spectra were observed in argon and krypton matrices with little difficulty. Whenever argon or krypton matrices were exposed to ultraviolet radiation from the $D_2$ lamp, the emission could be seen as a blue-green spot on the matrix which slowly faded away when the ultraviolet radiation was removed. In argon matrices the emission decayed very slowly and could be seen with the eye for 10 or 15 seconds after excitation ceased. In neon matrices, there was no detectable emission at wavelengths longer than the exciting light, which does not mean that no emission occurred, but rather implies that any emission which might have been excited was too weak to be detected by our experimental

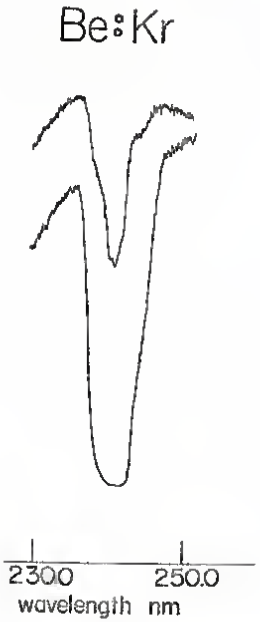


Figure 10. Ultraviolet absorption spectra of Be atoms in Kr matrices. The upper curve was recorded in a very dilute matrix. The lower curve was recorded in a matrix having a higher Be concentration.

apparatus. In both of the cases where emission was observed (argon and krypton), it was found that the emission spectrum was most intense when the output of the excitation monochromator (bandwidth = 1400 $cm^{-1}$) was centered on the $^1P_1 \leftarrow {}^1S_0$ Be atomic resonance transition for that particular matrix, and that as the exciting radiation was tuned away from the resonance energy, the emission intensity was diminished drastically. This observation confirmed that the emission process was specifically dependent on the population of the excited $2s2p\ {}^1P$ atomic state of beryllium.

The emission spectra were recorded with the excitation monochromator adjusted for maximum emission intensity for each experiment. The emission spectrum of Be in argon matrices showed an intensity maximum at 465.0 ± 0.1 nm (21 499 $cm^{-1}$) with a shoulder on the red side. The observed emission spectrum in argon is shown in Figure 11, uncorrected for photomultiplier response (S - 4) or monochrometer function. In krypton matrices the emitted light had an intensity maximum at 464.7 ± 0.1 nm (21 513 $cm^{-1}$) with a secondary emission peak at 517.0 ± 0.5 nm (19 337 $cm^{-1}$). The uncorrected krypton matrix emission spectrum is shown in Figure 12.

The decay time, $\tau$, for a system which obeys first order kinetics is defined by the relation

$$I(t) = I_o \exp(-t/\tau) \qquad (1.1)$$

where t is the time after excitation stops, I(t) is the emission intensity in arbitrary units at time t, and $\tau$ is the

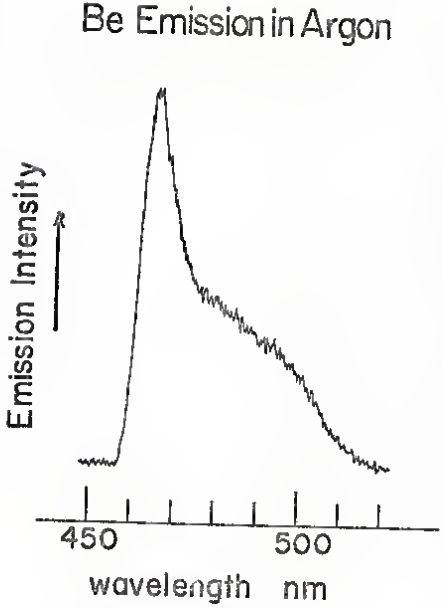


Figure 11. Spectrum of the long-lived emission observed in a Be doped Ar matrix.

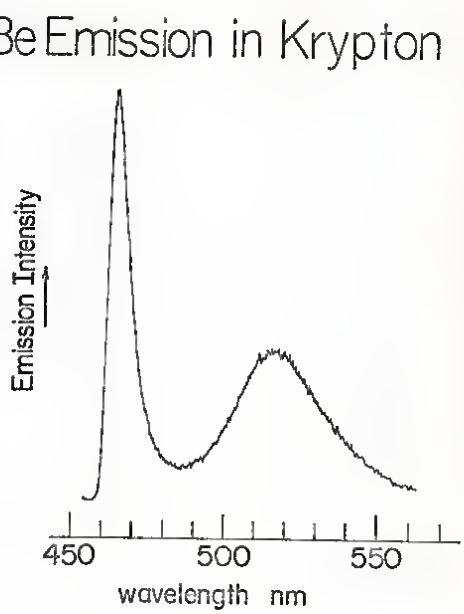


Figure 12. Emission spectrum of Be isolated in a Kr matrix. The emission was excited in the region of the $^1P \leftarrow {}^1S$ atomic absorption.

decay time, or the time for the emission intensity to fall to 1/e of its original value. If equation (1.1) is rearranged, we have

$$I(t)/I_o = \exp(-t/\tau) \quad . \qquad (1.2)$$

Then, taking the natural logarithm of both sides of equation (1.2) we have

$$\ln(I(t)/I_o) = -t/\tau \quad . \qquad (1.3)$$

So, a plot of $\ln(I(t))$ versus t should give a straight line whose slope is $-(1/\tau)$. Individual decay times were determined graphically from the slope of logarithm of intensity versus time plots, which are shown in Figures 13-15.

As nearly as can be determined the initial decay of all of the bands which were recorded appears to be exponential. Since the decay curves appear to be exponential, and since the high signal/noise points at short times after the excitation ceased were more heavily weighted in the graphical determination of the decay time, the reported values are representative of an initial decay obeying an assumed first order rate law, and will frequently be referred to as emission lifetimes.

The emission lifetime in argon matrices was found to be 1.33 ± 0.08 sec when measured at the wavelength of peak emission intensity. In krypton it was found that the two emission bands decayed with different lifetimes. The peak at 464.7 nm had a lifetime of 95 ± 5 msec, and the peak at 517.0 nm decayed with a lifetime 230 ± 25 msec. The long wavelength

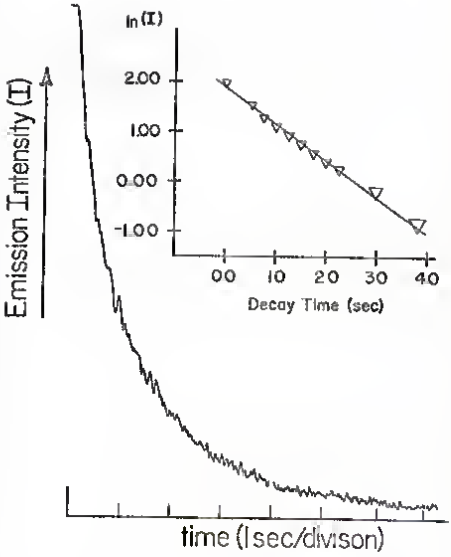


Figure 13. Decay curve for the 465 nm emission in Ar matrices.

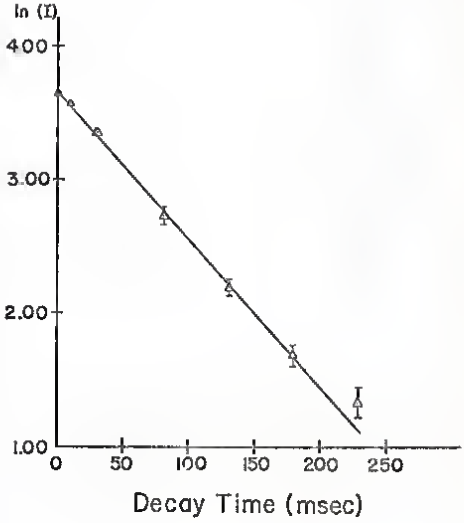


Figure 14. Plot of ln(Emission Intensity) vs. Time for the decay of the 465 nm emission in Kr matrices.

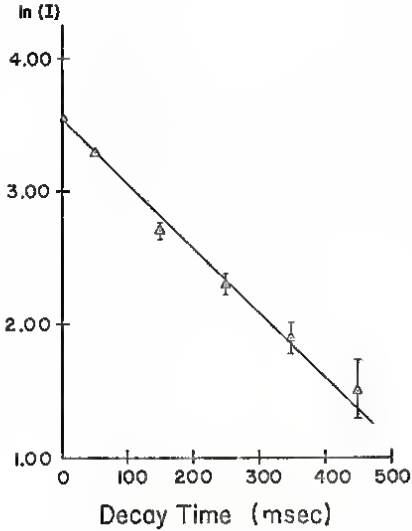


Figure 15. Plot of ln(Emission Intensity) vs. Time for the decay of the 517 nm emission in Kr matrices.

emission component was also found to diminish in intensity when the krypton matrix was annealed.

## Discussion

The Be atomic resonance line was observed in absorption in all three rare gas matrices. In neon this absorption was shifted to the blue of the gas phase absorption by 525 $cm^{-1}$. In argon and krypton the absorptions were red-shifted from the gaseous value by 205 and 998 $cm^{-1}$, respectively. Although no theory has yet been shown to accurately predict the shift of spectral absorption energies when going from the gas to the solid state, it has been recognized that with a few notable exceptions (charge transfer complexes), the observed shifts change in a regular fashion as the atomic weight of the host atom is changed. The trend is most easily identified when a guest atom is studied in a homologous series of hosts (such as the rare gases) where it is generally found to be true that an increase in the atomic weight of the host shifts the guest transition to lower energy. This effect (which is exemplified in the present work) has been explained in terms of the increasing van der Waals' forces between guest and host when the polarizability of the host is increased [39]. It was also found that the linewidth for the Be resonance absorption followed the trend Ne > Ar > Kr. This observation is consistent with other results [1] which have shown that atomic spectra are commonly sharpest in xenon and broader in argon and neon matrices.

The emission spectra which have been produced from Be metal in rare gas matrices suggest that we are dealing with at least three different atomic states in these experiments. It has been shown that the emission is from a state which is at most 21 500 $cm^{-1}$ above the ground state and that production of the emission is contingent upon absorption of light corresponding in energy to the $^1P \leftarrow {}^1S$ atomic transition, a quantum of energy of about 42 500 $cm^{-1}$. The only Be atomic state between the $^1S$ ground state and the excited $^1P$ state is the $^3P$ state which lies 21 980 $cm^{-1}$ above the ground state [26]. Therefore, it is inferred that the emission results from excitation of the $^1P$ state by absorption from the $^1S$ state, followed by intersystem crossing to the $^3P$ state, and radiative decay from the $^3P$ state back to the ground state. These processes (intersystem crossing and phosphorescence) are spin forbidden and have not been observed for Be atoms in the gas phase where the probability of collisional de-excitation greatly exceeds the probability of radiative decay. In the solid state, the external heavy atom effect of the rare gas hosts makes the triplet-singlet transition more allowed and shortens the radiative lifetime. However, the influence of the neon environment on the mixing of singlet and triplet states is apparently not large since no emission was observed in that case.

The suggestion that the emitting state is the $^3P$ state of the Be atom is supported by the following experimental evidence: (1) the emitting state has a long lifetime, indicating

that the transition is forbidden; (2) the lifetime becomes progressively longer going from Kr to Ar to Ne (not observed); and (3) the relative emission intensity increases in the order Ne (no observable emission) < Ar < Kr. These observations are also in agreement with the values of the spin-orbit parameters ($\zeta$) of the rare gases which increase in the order Ne($-521\ cm^{-1}$) < Ar($-940\ cm^{-1}$) < Kr($-3\ 479\ cm^{-1}$) [40].

In brief, these forbidden transitions are increased in intensity because of mixing of the rare gas electronic states with the electronic states of the solute by exchange interactions. Since heavy atoms have strong spin-orbit coupling, solute states of different multiplicity are more strongly coupled in the heavy atom host than in the gas phase, thus increasing the "allowedness" and shortening the radiative lifetimes of spin forbidden transitions. Multiplicity forbidden radiationless transitions are also dependent on the mixing of different spin states and so the rates of intersystem crossing transitions are also increased by heavy atom solvents. The effects of external heavy atoms on radiative and radiationless transitions have been discussed by Robinson [40] and by Robinson and Frosch [41], respectively.

The resolution of two emission bands in Kr matrices is difficult to explain. Both bands were excited only when the matrix was irradiated in the region of the $^1P \leftarrow {}^1S$ atomic absorption energy, so that both peaks appear to arise from atomic Be. The fact that the low energy peak diminished in intensity when the matrix was annealed suggests that the long

wavelength emission may be due to solute-solute interactions in non-nearest neighbor sites. This explanation would imply the formation of $Be_2$ on annealing, which was observed, but it fails to account for the nearly equal areas under the two Kr emission peaks.

Another possible explanation would be to attribute the separated emission peaks as being split due to "site effects." Multiple trapping sites may be formed as a result of variations in the solvent cage of the host in the doped sample which change the guest environment (site symmetry, surface boundaries, or neighboring vacancies). However, the 2200 $cm^{-1}$ splitting is extraordinarily large to be accounted for by such effects.

A third possibility involves the theory of zero-phonon transitions [42] which was developed to explain the absorption and luminescence spectra of certain color centers in alkali halide crystals near 0°K, and has only recently been applied to the luminescence of impurity centers in rare gas solids [43].

Zero-Phonon Transitions

The spectroscopic study of impurities in media which are optically transparent over some spectral region of interest has contributed greatly to the understanding of the physical properties of solutions and the underlying microscopic interactions between solvent and solute in the systems. The presence of narrow-line features in vibrationally broadened optical

transitions is not uncommon and can be related to such well-known phenomena as pure electronic transitions in molecular spectra or the recoil-free Mossbauer line in γ-ray spectra, where relatively sharp line structures are observed in strongly broadened transitions. In the optical case, the transition of a guest to an excited electronic state results in a change in the spatial density of the guest's electron cloud which can be accommodated by accompanying changes in the degree and energy of solvation. So, the states in equilibrium after excitation will have different solvent-solute interactions from those in the ground state. According to the Franck-Condon principle, however, immediately after excitation the geometry in the excited state must be the same as it was in the ground state. Then, given time, the exciplex (excited complex) may relax to its new equilibrium configuration by means of expansion or contraction of the solvent cage or perhaps by reorientation of some solvent particles. The host motions which are involved in the relaxation of the exciplex appear as vibrational quanta (phonons) in the solvent phonon band. This extra energy must be supplied by the optical photon, resulting in a shift and broadening of the absorption peak. However, since the exciplex states are quantized there is a finite probability that no vibrational mode will be excited. This contributes a single "zero-phonon line" that is neither displaced nor broadened by the energy transfer to the lattice modes.

A zero-phonon transition consists of two parts in luminescence near 0°K, (1) a sharp zero-phonon line which does

not involve an exchange of vibrational energy with the matrix, and (2) a multiphonon sideband on the low energy side of the zero-phonon peak, consisting of transitions which are assisted by exchanging energy with the phonon band of the solid. Since the luminescence band for this type of transition is the mirror image of the absorption band [42], the necessary equations can be developed in terms of absorption processes and later applied to the emission process.

This treatment is based on the model of two nondegenerate electronic states which are linearly coupled to a single lattice coordinate, which may be a normal-mode coordinate, or a configuration coordinate representing the displacements of neighboring host particles. This model was first considered by Muto [44], Huang and Rhys [45], and Pekar [46,47]. Their calculations were later formalized by Lax [48] and O'Rourke [49]. Most recently Keil [50] has reviewed the linear coupling model both semiclassically and quantum mechanically and has extended the theoretical treatment to include quadratic coupling to lattice modes. His procedure is outlined below in a notation similar to his.

Linear coupling.--In the simplest version of this model two nondegenerate electronic states, $\phi_a$ and $\phi_b$, at the defect are assumed to couple linearly to a single normal coordinate, q, of the lattice. In the Born-Oppenheimer and Condon approximations (the validity of various approximations which are commonly made in theoretical studies of optical absorption by impurity centers in crystals has been examined by Lax [48],

who regards the adiabatic approximation as "exact" in this context), these electronic wavefunctions must satisfy

$$[T_E + U(r,X)]\phi_i(r,X) = E_i(X)\phi_i(r,X), \quad (1.4)$$

where $T_E$ is the electronic kinetic energy operator, r represents the electronic coordinates, and X represents the nuclear coordinates. $E_i(X)$ is the adiabatic (Born-Oppenheimer) potential in which the nuclei move and is also the energy eigenvalue of the adiabatic Hamiltonian for state i. $U(r,X)$ is representative of all the terms in the total Hamiltonian except for the nuclear and electronic kinetic energies.

The nuclear part of the adiabatic Hamiltonian gives

$$[T_N + E_i(X)]\phi_{i\gamma}(X) = \epsilon_{i\gamma}\phi_{i\gamma}(X), \quad (1.5)$$

where $T_N$ is the nuclear kinetic energy operator, $E_i(X)$ is the previously mentioned nuclear potential, and $\phi_{i\gamma}$ is the vibrational wave function for the ith electronic state with vibrational quantum number $\gamma$ and energy eigenvalue $\epsilon_{i\gamma}$.

The nuclear potential $E_g(X)$ for the ground state may be expanded in a Taylor series in the displacements of the nuclei from their equilibrium positions. After performing a normal-mode transformation, the adiabatic potential may be written as

$$E_g(X) = \sum_i \frac{1}{2} M_i \omega_{ia}^2 Q_i^2 , \quad (1.6)$$

where $Q_i$ is the normal coordinate and $M_i$ and $\omega_{ia}$ are the effective mass and the frequency of the ith normal mode respectively.

Our interest in this problem lies in the b ← a transition and so we need expressions for the vibrational potentials and wavefunctions for both states. In general, the excited state, b, will have a different symmetry and hence different $Q_i$ from those of the ground state. To overcome the difficulty of multidimensional integrals in the line shape equations, the adiabatic potential $E_b(X)$ is expanded in terms of the normal modes for the ground state.

$$E_b(X) = E_{ab} + \sum_i A_i Q_i + \frac{1}{2} \sum_i M_i \omega_{ib}^2 Q_i^2 + \sum_{i \neq j} V_{ij} Q_i Q_j \qquad (1.7)$$

$E_{ab}$ is the energy separation of the potential curves at Q = 0 (the value of the normal coordinate at the minimum of the ground state potential is defined to be zero).

In the approximation of linear coupling to a single lattice mode the summations in Eq. (1.7) give only single terms, and $\omega_a = \omega_b = \omega$. The potentials for the ground and excited states are then given by

$$E_a = \frac{1}{2} M\omega^2 q^2 \qquad (1.8a)$$

and

$$E_b = \frac{1}{2} M\omega^2 q^2 + E_{ab} + A\hbar(M\omega/\hbar)^{1/2} q, \qquad (1.8b)$$

where the single lattice mode is given by q, and A is a measure of the linear interaction which displaces the equilibrium position of the mode but does not change its frequency.

The idea of reducing the impurity atom-crystal interaction to an equation involving a single lattice mode was introduced by von Hippel [51] and Seitz [52] for localized impurity centers in solids. They considered the description of these centers on a configuration coordinate scheme, in analogy with molecular physics. The potential energy of the center can be plotted as a function of the positions of the surrounding atoms in a manner similar to the familiar potential energy versus internuclear distance plots for the electronic states of diatomic molecules. In the case of a "tight-binding" impurity atom (a well-localized center in which both the ground and excited states are confined to a region not much larger than the distance to the nearest neighbors), the most important interactions are expected to be with the nearest neighbors, and it is likely that only the radial motion of nearest neighbors would have a large effect on the impurity energy. Of the radial modes of the surrounding lattice, the in-phase breathing mode of the nearest neighbor cage should be the most important. This argument indicates that the problem might reduce to coupling to one important lattice mode and several other minor vibrations. Lax [48] has, in fact, shown that a description in terms of one coordinate is frequently possible even when many degrees of freedom are really involved.

The solutions to Eq. (1.5) for the ground state are

$$\phi_{a\alpha}(q) = \left[\frac{(M\omega/\hbar)^{1/2}}{\pi^{1/2}\, 2^{a}\, a!}\right]^{1/2} \exp\left[-\frac{1}{2}\rho^2\right] H_a(\rho), \quad (1.9)$$

where $\rho = (M\omega/\hbar)^{1/2}q$ and $H_\alpha(\rho)$ is a Hermite polynomial [53]. The ground state energies are given by

$$\varepsilon_a = (\alpha + \tfrac{1}{2})\hbar\omega \ . \qquad (1.10)$$

For the excited state, b, the constants in the linear part of the potential, $A\hbar\omega(M\omega/\hbar)^{1/2}q$ were chosen such that $[\hbar\omega(M\omega/\hbar)^{1/2}q]^2 = E_a$ allowing the solutions to Eq. (1.5) for the excited state to be written as a product of harmonic oscillator wavefunctions of the form:

$$\phi_{b\beta}(q) = \left[\frac{(M\omega/\hbar)^{1/2}}{\pi^{1/2}\,2^\beta\,\beta!}\right]^{1/2} \exp[-(\tfrac{1}{2})(\rho + A)^2]H_\beta(\rho + A)^2 \qquad (1.11)$$

with energies

$$\varepsilon_{b\beta} = (\beta + \tfrac{1}{2})\hbar\omega + E_{ab} - \frac{A^2}{2}\hbar\omega. \qquad (1.12)$$

Following Lax [48], and invoking the Condon approximation, the normalized line shape function for the transition b ← a may be written as

$$I_{ab}(E) = Av_\alpha \sum_\beta |\langle\phi_{a\alpha}|\phi_{b\beta}\rangle|^2 \delta(\varepsilon_{b\beta} - \varepsilon_{a\alpha} - E) \qquad (1.13)$$

where $Av_a$ is a thermal average over initial vibrational states and $\sum_\beta$ is a sum over the final vibrational states.

The overlap integral between displaced harmonic oscillator wavefunctions is

$$\int \phi_{a\alpha}(q)\,\phi_{b\beta}(q)\,dq = \langle\phi_{a\alpha}|\phi_{b\beta}\rangle, \qquad (1.14)$$

which has been shown [50] to be given by

$$\langle \phi_{aa} | \phi_{b\beta} \rangle = \exp\left(\frac{-A^2}{4}\right) \left(\frac{\alpha!}{\beta!}\right)^{1/2} \left(\frac{A}{2^{1/2}}\right)^{\beta-\alpha} L_{\alpha}^{\beta-\alpha}\left(\frac{A^2}{2}\right), \qquad (1.15)$$

where $L_n^m(a)$ is the Laguerre polynomial. For T = 0°K, only the ground vibrational state ($\alpha = 0$) is occupied. Using $L_o^m(z) = 1$, letting $\beta = \beta - a$, and setting $a = \frac{1}{2} A^2$, the normalized transition probability becomes

$$W_{o\beta} = e^{-S} \left(\frac{S^{\beta}}{\beta!}\right). \qquad (1.16)$$

The line shape function defined by Eq. (1.13) is

$$I_{ab}(E) = \sum_{\beta=0}^{\infty} e^{-S} \left(\frac{S^{\beta}}{\beta!}\right) \delta(\beta\hbar\omega + E_{ab} - S\hbar\omega - E) \qquad (1.17)$$

and consists of a series of evenly spaced $\delta$ functions at energies

$$E_{\beta} = (E_{ab} - S\hbar\omega) + \beta\hbar\omega = E_o + \beta\hbar\omega \qquad (1.18a)$$

for absorption and

$$E_{\beta} = E_o - S\hbar\omega \qquad (1.18b)$$

for emission, where $\hbar\omega$ is the average phonon energy of the solid host. The line shape function reaches a maximum at $\beta \approx S$ and declines for higher values of $\beta$. The zero phonon transition at $E_o$ has the normalized probability

$$W_{oo} = e^{-S}. \qquad (1.19)$$

Keil [50] has calculated the line shape function for the multiphonon bands semiclassically and quantum mechanically

for different values of the coupling constant S. Figure 16 shows the calculated relative intensities of the quantum mechanical delta functions and the semiclassical line shapes for the multiphonon band envelopes. In those cases where the individual components of the line series are not resolved, the multiphonon band may be described in terms of the moments of the distribution function of Eq. (1.17). The first few of these, given by Lax [48], are

$$M_0 = \sum_{\beta=0}^{\infty} W_{0\beta} = 1 \qquad (1.20a)$$

$$M_1 = \sum_{\beta=0}^{\infty} W_{0\beta} E_\beta = E_0 \pm S\hbar\omega = \bar{E} \qquad (1.20b)$$

$$M_2 = \sum_{\beta=0}^{\infty} W_{0\beta} (E_\beta - \bar{E})^2 = S(\hbar\omega)^2 \coth(\hbar\omega/2kT) \qquad (1.20c)$$

where for $M_1$ the plus and minus signs refer to absorption and emission, respectively. If only the multiphonon band is considered for a system with $S >> 1$ at 0°K, then the second moment of the distribution function, which is equal to the square of the standard deviation ($\sigma$) for the distribution, gives directly a value for $S(\hbar\omega)^2$ since $\lim_{x\to\infty} \coth(x) = 1$.

A more direct way to get a number for $S(\hbar\omega)^2$ is through the more easily measured fwhm (full width at half maximum) of the multiphonon absorption or emission band. Assuming a Gaussian line shape function it is easily shown using tabulations for the normal probability function and related functions [54] that

$$\text{fwhm} = 2.36\sigma = 2.36\, M_2^{1/2} = 2.36\, S^{1/2}\hbar\omega \,. \qquad (1.21)$$

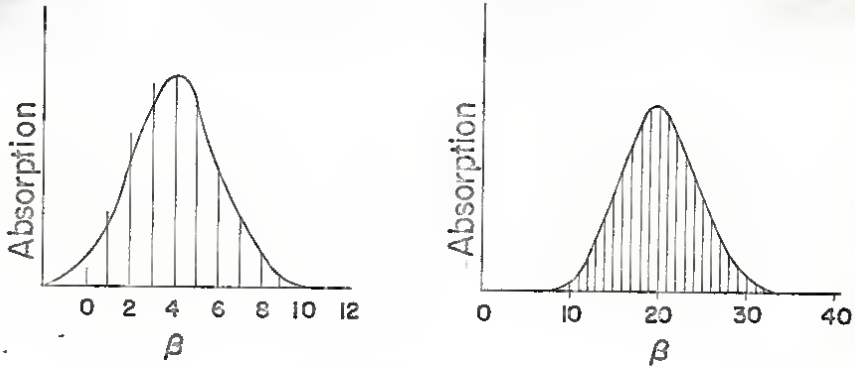


Figura 16. Calculated relative intensities of the quantum mechanical delta functions (vertical lines) and the semiclassical line shapes (continuous curves) for the multi-phonon band envelopes, after Keil [50]. The left hand plot is for the weak coupling, $\beta = 4$ case. The plot on the right is for the case showing strong coupling, $\beta = 20$.

Knowing that the multiphonon sideband is peaked around $\beta = S$, we have from Eq. (1.18b)

$$E_{\beta=S} - E_o = S\hbar\omega \tag{1.22}$$

and combining with Eq. (1.21) gives

$$\frac{E_S - E_o}{S} = \hbar\omega = \frac{(\text{fwhm})}{2.36\ S^{1/2}} \tag{1.23}$$

and

$$S = \left(\frac{(E_S - E_o)}{(\text{fwhm})}\ (2.36)\right)^2. \tag{1.24}$$

Then S can be calculated from the measured fwhm for the multiphonon sideband, and knowing S, $\hbar\omega$ can be determined.

Application of linear coupling to Be in Kr.--For the beryllium emission in krypton matrices the fwhm is easily measured and is found to be 0.09 eV. This gives a value for S of about 53, and $\hbar\omega \cong 5.3$ meV $\cong 42\ cm^{-1}$. This value of $\hbar\omega$ can be favorably compared with the values obtained from neutron scattering measurements in krypton [55] of 4 to 6 meV and with an experiment similar to this one involving a zero phonon emission spectrum of oxygen atoms in solid krypton [43] which gave a value of 5 meV for $\hbar\omega$.

The intensity of the zero phonon emission peak in this system is observed to be rather large, as was the case for oxygen atoms in solid krypton [43]. The noted decrease in intensity of the multiphonon sideband relative to the zero phonon peak as the matrix was annealed may indicate that the

matrix as initially formed contained beryllium trapped in several different sites, the most stable of which was not coupled to the lattice as strongly as the site which decreased in intensity when annealed. The absence of an observable multiphonon sideband on the high energy side of the $^1P \leftarrow {}^1S$ atomic absorption in the matrix certainly suggests that the $^3P$ atomic state is coupled more strongly to the lattice than either the $^1P$ or $^1S$ states. It is also obvious from the proximity of the sideband to the zero phonon band in the argon emission spectra that the coupling to the rare gas lattice is weaker in that matrix than in krypton. This, of course, is also evident in the emission lifetime trends which indicate greater impurity-host interactions in krypton than in argon.

Other Observed Transitions

In argon the absorption bands at 270.8 and 262.2 nm were only observed when radiation below 240 nm excited the sample. From this information and knowing that the lowest $^3P$ state is significantly populated under these conditions, these absorptions are tentatively assigned as triplet-triplet transitions of the Be atom. (This possibility was suggested earlier by Brewer and Wang [10] in their $Mg_2$ work to account for some absorption bands in the region of 359 nm in Kr. However, they did not succeed in showing that the $^3P$ state of Mg was populated or needed to be populated for the transitions to be observed.) It is possible that the bands may be

associated with the $2p^2\ ^3P \leftarrow 2s2p\ ^3P$ transition which occurs at 265.0 nm in the gas phase. These weak absorptions were only observed in highly concentrated matrices, and they weakened considerably on annealing, as the $Be_2$ bands intensified. It is assumed that after annealing, the Be atom concentration had decreased, and the narrowed resonance linewidth reduced the steady state concentration of atoms in the $^3P$ state.

It is also tempting to assign the doublet at 216.2 and 217.2 nm as the $2s4d\ ^3D \leftarrow 2s2p\ ^3P$ transition which occurs at 217.5 nm in the gas phase. A difficulty with this assignment is that these bands do not appear to weaken on annealing in the same manner as the 270.8 and 262.6 nm bands. Neither can we rule out $Be_2$ or higher Be polymers as the source of these absorptions.

## Summary

Beryllium atoms were trapped in neon, argon, and krypton matrices near 4°K and studied via absorption spectroscopy in the far ultraviolet spectral region. Absorptions which are assignable to the $^1P_1 \leftarrow {}^1S_0$ atomic resonance transition were recorded along with some weaker bands which are tentatively assigned to "pumping transitions" within the triplet manifold of the beryllium electronic states. Long-lived emission bands were also observed in the visible region at a wavelength of about 465 nm in argon and krypton matrices,

which were assigned to the $^3P \rightarrow {}^1S$ atomic phosphorescence transition (not previously observed) and interpreted in terms of a model which introduces a linear interaction between the matrix material and the trapped species in the Hamiltonian for the system.

The work done here on atomic beryllium suggests that experiments using high power, ultra-fast light sources and fast spectroscopic recording devices might give greater insight into the solvent-solute interactions in the doped matrix by examination of the time-resolved emission spectra for energy shifts as a function of time after excitation. This type of experiment has not been reported for matrix isolated compounds as yet, though it has been successfully employed in liquid solutions and pure solids, and it does appear to hold great promise for future work in this area. Another experiment which is suggested by this work is the reexamination of magnesium atoms in argon, krypton, and xenon to search for emission spectra analogous to those observed here for beryllium. The corresponding $^3P_1 \rightarrow {}^1S_0$ absorption has recently been used in the gas phase to populate the triplet state which was found to decay with a lifetime of 2.2 msec [56], and the fact that the rates for these processes are known in the gas phase should permit a more complete interpretation of the intersystem crossing and radiative rate processes in the trapped impurity state to be made.

REFERENCES, CHAPTER I


1. A review of the optical spectroscopy of atoms in solid matrices may be found in F. Meyer, Low Temperature Spectroscopy (American Elsevier, New York, 1971).

2. E.E. Merrithew, G.V. Marusak, and C.E. Blount, J. Mol. Spectry 29, 54 (1969).

3. W. Weyhmann and F.M. Pipkin, Phys. Rev. 137, A490 (1965).

4. S.L. Kupferman and F.M. Pipkin, Phys. Rev. 166 (2), 207 (1968).

5. F. Meyer, J. Chem. Phys. 43, 2986 (1965).

6. L. Brewer, E.A. King, J.L. Wang, F. Meyer, and G.F. Moore, J. Chem. Phys. 49, 5209 (1968).

7. L. Andrews and G.C. Pimentel, J. Chem. Phys. 47, 2905 (1967).

8. O. Schnepp, J. Phys. Chem. Solids 17, 188 (1961).

9. M. Brith and O. Schnepp, J. Chem. Phys. 39, 2714 (1963).

10. L. Brewer and J.L. Wang, J. Mol. Spectry. 40, 95 (1971).

11. R.L. Barger and H.P. Broida, Nat. Bur. Std. (U.S.) Rep. 8200 (1963).

12. J.E. Francie, Jr. and S.E. Webber, J. Chem. Phys. 56, 5879 (1972).

13. W.W. Duley and W.R.M. Graham, Nature 224, 785 (1969).

14. W.R.M. Graham and W.W. Duley, Nature Phys. Sci. 232, 43 (1971).

15. M. Guy, J.-Y. Roncin and N. Damany, Compt. Rend. 263B, 546 (1966).

16. W.W. Duley, Proc. Phys. Soc. (London) 91, 976 (1967).

17. M. McCarty, Jr. and G.W. Robinson, Mol. Phys. 2, 415 (1959).

18. K. Dressler, J. Opt. Soc. Am. 50, 501 (1960).

19. L. Brewer, B. Meyer, and G.D. Brabson, J. Chem. Phys. 43, 3973 (1965).

20. W.W. Duley, Proc. Phys. Soc. (London) 90, 263 (1967).

21. J.-Y. Roncin, N. Damany and J. Romand, J. Mol. Spectry. 22, 154 (1967).

22. J.S. Shirk and A.M. Bass, J. Chem. Phys. 49, 5156 (1968).

23. L. Brewer and B. King, J. Chem. Phys. 53, 3981 (1970).

24. L. Brewer, C. Chang and B. King, Inorg. Chem. 9, 814 (1970).

25. W.W. Duley, Proc. Phys. Soc. (London) 92, 830 (1967).

26. C.E. Moore, Atomic Energy Levels, NBS Circular 467 vol. 1 (1949).

27. F. Paschen and P.G. Krugar, Ann. der Phys. 8, 1005 (1931).

28. F. Paschen, Ann. der Phys. 12, 514 (1932).

29. B. Edlan, Nova Acta Reg. Soc. Sci. Uppsala (IV) 9, No. 6, 51 (1934).

30. W.F. Meggers, J. Opt. Soc. Am. 36, 431 (1946).

31. T. Anderson, K.A. Jessan and G. Sorensan, Phys. Rev. 188, 76 (1969).

32. R.F. Paton and R.E. Nusbaum, Phys. Rev. 33, A1093 (1929).

33. W. Weltner, Jr., P.N. Walsh, and C.L. Angell, J. Chem. Phys. 40, 1299 (1964).

34. W. Weltner, Jr. and D. McLeod, Jr., J. Chem. Phys. 45, 3096 (1966).

35. H.A. Jones, Phys. Rev. 28, 202 (1926).

36. W. Espe, Materials of High Vacuum Technology, vol. 1, pp. 46-48 (Pergamon Press, Oxford, 1966).

37. J. Schubart, Sci. American 199 (2), 27 (1958).

38. M.I. Sax, Dangerous Properties of Industrial Materials (Van Nostrand Reinhold Company, New York, 1968).

39. H.C. Longuet-Higgins and J.A. Pople, J. Chem. Phys. 27, 192 (1957).

40. G.W. Robinson, J. Mol. Spectry. 6, 58 (1961).

41. G.W. Robinson and R.P. Frosch, J. Chem. Phys. 38, 1187 (1963).

42. D.B. Fitchen in Physics of Color Centers, W.B. Fowler, Ed., (Academic, New York, 1968), chapter 5.

43. W.F. Lewis and K.J. Teegarden, Phys. Rev. B 8, 3024 (1973).

44. T. Muto, Progr. Theoret. Phys. (Kyoto) 4, 181 (1949).

45. K. Huang and A. Rhys, Proc. Roy. Soc. (London) A204, 406 (1950).

46. S. Pekar, Zh. Eksperim. i Teor. Fiz. 20, 510 (1950).

47. S. Pekar, Uspekhi Fiz. Nauk. 50, 193 (1953).

48. M. Lax, J. Chem. Phys. 20, 1752 (1952).

49. R.C. O'Rourke, Phys. Rev. 91, 265 (1953).

50. T.H. Keil, Phys. Rev. 140, A601 (1965).

51. A. von Hippel, Z. Physik 101, 680 (1936).

52. F. Seitz, Trans. Faraday Soc. 35, 79 (1939).

53. Albert Messiah, Quantum Mechanics, vol. 1, Appendix B, (John Wiley and Sons, Inc., New York, 1966).

54. S.M. Selby, Editor-in Chief, CRC Standard Mathematical Tables, 17th edition, p. 579 (The Chemical Rubber Co., Cleveland, Ohio, 1969).

55. W.B. Daniels, G. Shirane, B.C. Frazer, H. Umebayashi, and J.A. Leake, Phys. Rev. Lett. 18, 548 (1967).

56. J.J. Wright, J.F. Dawson, and L.C. Balling, Phys. Rev. A 9, 83 (1974).

CHAPTER II

# OPTICAL SPECTROSCOPY OF BERYLLIUM DIMERS IN RARE GAS MATRICES

## Introduction

In the past, experimental efforts to detect $Be_2$ in the gas phase have been unsuccessful [1-3], although at the higher temperatures which were investigated the predicted equalibrium concentration is one hundred parts per million [4]. These results indicate that the beryllium dimer is a very weekly bound molecule in its ground state as are all the group IIA metal dimers which have been observed. Since these molecules exhibit no true chemical bond in the usual sense of the term, their binding energy has been explained in terms of the week interatomic or intermolecular interactions which are typical of so-called van der Waals molecules and which include dispersion forces, hydrogen bonding, and electric multipole interactions. These forces lead to bond energies for van der Waals molecules which are typically hundreds of times less than the energies of ordinary chemical bonds. As a result of these extremely low bond energies, even at low temperatures where the kinetic energy and the depth of the van der Waals potential well are comparable, less than 1 percent of the gas will be in the form of dimer at pressures of 1 atmosphere. A further decrease in temperature

at constant monomer concentration will increase the dimer concentration, but below the condensation point vapor pressures decrease very rapidly and the dimer concentration which is proportional to the square of the monomer concentration must also drop significantly. These observations suggest that equilibrium techniques are frequently unsuitable for the generation of van der Waals molecules and that non-equilibrium techniques should be investigated.

Matrix isolation has been proved to be a successful method for the production of van der Waals molecules. The molecules are produced by annealing a matrix of isolated monomer or by depositing the monomer at a rate which is high enough for dimers to be formed on the matrix surface as it solidifies. A difficulty with this technique is that interactions with the surrounding matrix particles may be comparable to the bond strengths of the weakest van der Waals molecules leading to significant structural differences between the matrix isolated molecule and the molecule in the gas phase. Good results have been obtained with the homonuclear dimers of metals in rare gas matrices. Of the Group IIA metals, $Mg_2$ and $Ca_2$ have been identified in the gas phase [5,6] as well as in rare gas matrices [7,8]. In this work an absorption spectrum assignable to the $Be_2$ molecule has been observed for the first time and analyzed to give structural information about the excited state populated by the absorption.

## Experiments and Observations

The experiments were the same as for the atomic absorption of beryllium atoms in rare gas matrices and are described in Chapter I. The only change was that higher Be concentrations were used in the parts of the experiments involving the dimers. As the concentration of Be in the matrix was increased, absorption features assigned to beryllium aggregates were observed in neon, argon, and krypton. Although the range from 685 to 199 nm was scanned, no bands were seen at wavelengths longer than 370 nm.

A progression of discrete bands assignable to $Be_2$ was observed in the region from 370 to 320 nm in neon and argon matrices with separations of about 450 $cm^{-1}$ between adjacent peaks (see Figures 17 and 18). This assignment is substantiated by the facts that $Be_2$ is the most probable initial aggregate to be seen upon annealing a matrix doped with Be atoms: the bands appear to exhibit a single vibrational progression; no known diatomic molecule containing Be has a vibrational frequency as low as 500 $cm^{-1}$; and the work of Brewer and Wang [7] on Mg has demonstrated the formation of homonuclear diatomics from Group IIA metals in rare gas matrices. Since the equilibrium concentration of $Be_2$ in the gas phase has been shown to be negligible at these temperatures [4], it is assumed that the dimer is formed during the condensation process on the matrix surface. This mechanism is consistant with the experimental difficulty in producing $Be_2$ in krypton matrices and with the observed annealing

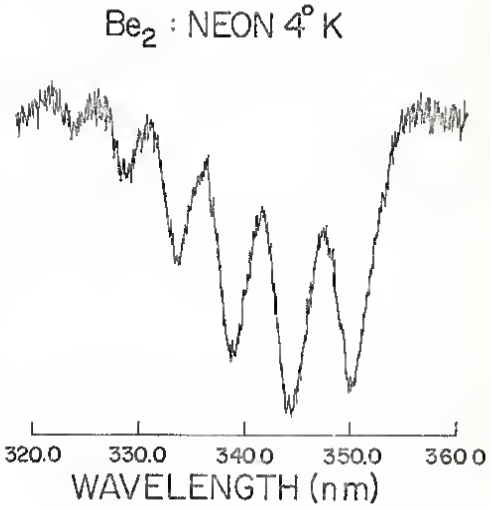


Figure 17. Ultraviolet absorption spectrum of $Be_2$ in an Ne matrix.

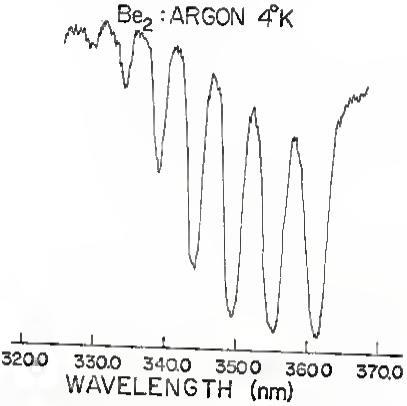


Figure 18. Ultraviolet absorption spectrum of $Be_2$ in an Ar matrix.

properties of the different rare gas solids containing Be atoms.

The $Be_2$ bands, as shown in Figures 17 and 18, exhibited a matrix shift of about 900 $cm^{-1}$ to the blue when going from argon to neon. This is at least qualitatively consistent with most observations on molecular electronic transitions in these two matrices. Also consistent with matrix effects in these solids is the shift in vibrational frequency in the upper state from 489 $cm^{-1}$ in neon (Table 2), where the trapped molecule is usually considered to be in the more gas-like environment, to 474 $cm^{-1}$ in argon (Table 3). However, the line widths in Ne were approximately 400 $cm^{-1}$ fwhm as compared to about 250 $cm^{-1}$ in argon, indicating more, or at least a larger range of solute-solvent interaction in the former matrix.

The spectra in krypton showed some weak, ill-defined bands in the region of 350 nm when very high concentrations of Be were used (see Table 1), but it appears that $Be_2$ is only formed in krypton matrices with great difficulty, even after the matrix is warmed to allow diffusion to occur.

The $Be_2$ spectra in Ne and Ar show slightly different intensity distributions. The assignments of the (0,0) bands follow from the absence of any absorption to the red of the longest wavelength band and from the shapes of the band envelopes. Since the ground state of $Be_2$ is expected to be stabilized only by van der Waals interactions between the atoms, a relatively large interatomic distance is implied.

TABLE 2

ABSORPTION BANDS OF $A^1\Sigma_u^+ \rightarrow X^1\Sigma_g^+$ of $Be_2$ IN A NEON MATRIX AT 4°K

| $(v',v'')$ | $\lambda_{air}$(nm) | $\nu_{vac}$($cm^{-1}$) | $\Delta G'_{v+1/2}$($cm^{-1}$) |
|---|---|---|---|
| (0,0) | 350.15 ± 0.05 | 28 551 | |
| | | | 489 |
| (1,0) | 344.25 ± 0.05 | 29 040 | |
| | | | 476 |
| (2,0) | 338.7 ± 0.05 | 29 516 | |
| | | | 460 |
| (3,0) | 333.5 ± 0.10 | 29 976 | |
| | | | 477 |
| (4,0) | 328.6 ± 0.20 | 30 423 | |
| | | | 460 |
| (5,0) | 323.7 ± 0.40 | 30 883 | |

TABLE 3

ABSORPTION BANDS OF $A^1\Sigma_u^+ \leftarrow X^1\Sigma_g^+$ of $Se_2$ IN AN ARGON MATRIX AT 4°K

| $(v',v'')$ | $\lambda_{air}$ (nm) | $\nu_{vac}$ ($cm^{-1}$) | $\Delta G'_{v+1/2}$ ($cm^{-1}$) |
|---|---|---|---|
| (0,0) | 361.30 ± 0.05 | 27 670 | |
| | | | 474 |
| (1,0) | 355.21 ± 0.05 | 28 144 | |
| | | | 467 |
| (2,0) | 349.41 ± 0.05 | 28 611 | |
| | | | 455 |
| (3,0) | 343.95 ± 0.07 | 29 066 | |
| | | | 447 |
| (4,0) | 338.74 ± 0.07 | 29 513 | |
| | | | 436 |
| (5,0) | 333.8 ± 0.10 | 29 949 | |
| | | | 437 |
| (6,0) | 328.9 ± 0.10 | 30 386 | |

The transition to a bonding excited state (as evidenced by the observed vibrational progression) should lead to a decrease in interatomic distance and an extended Franck-Condon envelope, as in $Mg_2$ [7]. However, it does appear here that the $\Delta r$ between ground and excited states is considerably less for $Be_2$ than for $Mg_2$. One expects the matrix to have a more pronounced effect on the weakly bound ground state than on the bonded excited state for these molecules, so that any change in bond length attributable to matrix interactions would probably appear in the ground electronic state. Assuming that the ground state bond length is always greater than the bond length in the $A^1\Sigma_u^+$ excited state, this argument would explain the difference in the shapes of the absorption envelopes for $Be_2$ in neon and argon in terms of a change in $r_{Be-Be}$ in the $X^1\Sigma_g^+$ state, going from a value in argon which is approximately equal to $r_{Be-Be}$ in the excited state to a slightly larger value in neon. The resulting change in the relative positions of the potential energy curves of the electronic states would alter the Franck-Condon factors for the transition and lead to the different band shapes, as observed.

When the argon matrices were allowed to warm up the $Be_2$ bands could be seen to grow in intensity as the matrix slowly evaporated, indicating the dimerization of Be atoms in the matrix. In neon, a striking increase in the rate of dimerization was observed: one of the neon experiments was done in a dewar which is used primarily for ESR work [9], where the trapping surface is a 2 mm diameter sapphire rod

cooled to 4°K. After the first deposit, the spectra showed strong Be atom absorption and no $Be_2$ bands. A second deposit was made at a higher temperature in hopes of increasing the Be concentration and observing $Be_2$. After the second deposit strong $Be_2$ bands were observed, but the Be atomic absorption had disappeared. This is interpreted as showing that as the matrix warmed during the second deposit, most of the Be atoms diffused through the neon matrix and aggregated as $Be_2$ molecules.

These observations can be rationalized by consideration of the van der Waals interactions between Be atoms and between Be atoms and the surrounding matrix particles. If there is no valence attraction, the attractive potential between two neutral atoms, A and B, in S states may be written as $-C_{AB}/r^6$, where $C_{AB}$ is a constant for the pair of atoms under consideration. Shabanova [10], using oscillator strengths of the spectral lines of the atoms, has calculated the $C_{AB}$ constants of the van der Waals interactions of Be with the rare gases and with itself. His calculated values are listed in Table 4 and indicate that the Be-Be attractive potential exceeds the Be-rare gas attractive potential in all three cases. The Ne case, however, shows an extraordinary increase in the relative magnitudes of the Be-Be and Be-rare gas potentials. This parallels the observation that only in neon was there a dramatic increase in the dimer concentration and decrease in the atom concentration when the matrix was warmed. It also offers an explanation of

TABLE 4

$C_{AB} \cdot 10^{60}$, erg · cm$^6$

| Atom | Ne | Ar | Kr | Be |
|---|---|---|---|---|
| Be | 23.6 | 91.3 | 130.0 | 210.0 |
| $\frac{C_{BeBe}}{C_{BeR}}$ | 8.9 | 2.3 | 1.6 | 1.0 |

the difficulty in producing $Be_2$ in krypton matrices. The difference in attractive potentials is so small that in the short time that the Be atoms are mobile on the matrix surface, they are not able to distinguish another Be atom in the potential fields of the surrounding Kr atoms. Also, of course, in the preparation of the matrices the fact that the triple point of Kr is 32° higher than Ar and 91.2° higher than Ne will reduce the time required for solidification at the Kr surface and lead to less initial formation of $Be_2$.

## Assignment of $Be_2$ Bands

It appears most likely that the observed matrix systems with (0,0) bands at 28,551 $cm^{-1}$ in neon and 27,670 $cm^{-1}$ in argon (Tables 2 and 3) correspond to the $A^1\Sigma_u^+ \leftarrow X^1\Sigma_g^+$ transition of $Be_2$. Since the frequencies for other molecules observed in these two matrices usually bracket the gas phase value, one might then expect to observe this transition at about 28,000 $cm^{-1}$ in the gas phase. The configurations involved in these two states and in other low-lying excited states are approximately as follows:

i) $KK(\sigma_g 2s)^2(\sigma_u 2s)^2$ $\quad X^1\Sigma_g^+$

ii) $KK(\sigma_g 2s)^2(\sigma_u 2s)(\sigma_g 2p)$ $\quad {}^1\Sigma_u^+,\ {}^3\Sigma_u^+$

iii) $KK(\sigma_g 2s)^2(\sigma_u 2s)(\pi_u 2p)$ $\quad {}^1\Pi_g,\ {}^3\Pi_g$

iv) $KK(\sigma_g 2s)(\sigma_u 2s)^2(\pi_u 2p)$ $\quad {}^1\Pi_u,\ {}^3\Pi_u$

v) $KK(\sigma_g 2s)(\sigma_u 2s)^2(\sigma_g 2p)$ $\quad {}^1\Sigma_g^+,\ {}^3\Sigma_g^+$ .

The $(\sigma_u 2s)$ orbital is antibonding and the $(\sigma_g 2s)$, $(\sigma_g 2p)$, and $(\pi_u 2p)$ orbitals are bonding. The lowest state, given by configuration i), has an equal number of bonding and antibonding electrons and is predicted to be repulsive by simple molecular orbital theory. In fact, this state has been predicted to be repulsive by every theoretical calculation made and published for the $Be_2$ molecule [11-15]. Molecular orbital calculations, while useful in predicting the properties of conventional chemical bonding forces at small internuclear distances, have been for the most part unsuccessful in determining the effects of weak, long-range van der Waals forces. As a result of these weak attractive forces, the ${}^1\Sigma_g^+$ state arising from configuration i) may be expected to have a shallow potential well similar to $Mg_2$ [5] and $Ca_2$ [6] which have been previously shown to be bound in their ground states. At the low temperature of these experiments, it is fair to assume that only the ground state of this molecule is significantly populated and that the observed transition originates from this $X\,{}^1\Sigma_g^+$ electronic state.

It is difficult to predict whether configuration ii) or iii) lies lower in energy, but of the electronic states formed from these configurations only the ${}^1\Sigma_u^+$ can combine strongly with the ground state. Of the remaining higher energy configurations only the ${}^1\Pi_u$ state derived from configuration iv) should combine strongly with the ground state.

In $Mg_2$ the gas phase spectrum has been observed and analyzed by Balfour and Douglas [5]. There the $A\,^1\Sigma_u^+ \rightarrow X\,^1\Sigma_g^+$ transition occurs at 26 150 $cm^{-1}$. The transition to the A state of $Mg_2$ has been observed by Brewer and Wang [7] in Kr (and Xe) matrices where it presents a broad, symmetric Franck-Condon envelope extending from 396 nm (25 230 $cm^{-1}$) to 374 nm (26 740 $cm^{-1}$) so that, as those authors point out, an unambiguous assignment of the (0,0) transition cannot be made without further experimental evidence.

Another similar molecule in which the $^1\Sigma_u^+$ state has been definitely assigned as the A state is $Ca_2$. Balfour and Whitlock [6] have studied this molecule in the gas phase where the A → X transition occurs at 19 401 $cm^{-1}$. Francis and Webber [8] have made a tentative assignment to a transition seen at 18 002 $cm^{-1}$ in krypton matrices doped with Ca as being the A → X transition of the $Ca_2$ molecule. Hence the position of the observed $Be_2$ system is in agreement with an expected shift to higher energies for this transition as the metal diatomic becomes lighter. However, the calculations of Bender and Davidson [15] do not appear to support this assignment but, on an energy basis, would rather assign the observed system of $Be_2$ to the $^1\Pi_u - X\,^1\Sigma_g^+$ transition where the upper state formally results from the $(\sigma_g 2s)(\pi_u 2p) + (\sigma_g 2s)^2$ excitation. This is because those authors find the $^1\Pi_u$ and $^1\Sigma_u^+$ states to lie about 27 000 and 36 000 $cm^{-1}$ above the ground state, respectively. However, it has been suggested by Balfour and Douglas that bands in the $Mg_2$ spectrum at about

36 000 $cm^{-1}$ arise from a transition to the $^1\Pi_u$ state, so that there, as expected from orbital energy considerations, the $^1\Pi_u$ state would lie considerably higher than the $^1\Sigma_u^+$.

A discussion of $Be_2$ with Professor Davidson [16] indicates that the disagreement might not be as great as the calculated values [15] indicate since the accuracy of the energy-level computation is considered to be about ± 1 eV. Also, the $^1\Pi_u$ state is found by them to contain a large amount of the $(\sigma_g 2p)(\pi_u 2p)$ configuration in which case the $^1\Pi_u \rightarrow X^1\Sigma_g^+$ transition would involve a two electron transition and therefore be weak. They expect interatomic distances to be calculated well by their model and the distance in the $^1\Pi_u$ state (about 3.5 $a_o$) is considerably shorter than in the $\Sigma$ states (about 4.5 $a_o$) indicating that the $^1\Pi_u \rightarrow X^1\Sigma_g^+$ transition would be further weakened by the Franck-Condon effect. It is then expected, from this and other approximate calculations [17] that the $^1\Sigma_u^+ \rightarrow X^1\Sigma_g^+$ transition would be the most intense. Since there is only one molecular transition observed in matrices and there is no basic disagreement with Bender and Davidson's calculation, we assign our observed systems to the $A^1\Sigma_u^+ \rightarrow X^1\Sigma_g^+$ transition of $Be_2$.

## Discussion

The molecular states which can be formed by the combination of a Be atom in the $^1S$ state with another Be atom in the $^1P$ state are given by the singlet terms of configurations (ii)-(v) listed above. Consequently, the dissociation limit

of these molecular states should correspond to the sum of the energies of the separated atoms ($^1S + {}^1P$). Figure 19 shows schematically the energy relationships between the atomic and molecular states for the $Be_2$ molecule. The ground state, $^1\Sigma_g^+$, must dissociate into a pair of ground state Be atoms. The work required to perform this separation on a $Be_2$ molecule from the lowest vibrational level of its potential energy well is symbolized by $D_o''$ (probably greatly exaggerated in the figure). For the $^1\Sigma_u^+$ state, $D_o'$ is indicated in the figure as the depth of the lowest vibrational level ($v' = 0$) in the potential well below the ($^1S + {}^1P$) separated atom energies. It is easily seen that the difference between these two dissociation limits is just the energy necessary for the atomic transition $^1P \rightarrow {}^1S$ and that the dissociation energy of the upper state is given to a good approximation by

$$D_o'(^1\Sigma_u^+) = \bar{\nu}_{^1P \rightarrow {}^1S}(Be) + D_o''(^1\Sigma_g^+) - \bar{\nu}_{00}(Be_2).$$

Using the observed transition energies in an argon matrix and neglecting $D_o''$ yields

$$D_o'(^1\Sigma_u^+) = 42{,}360\ cm^{-1} - 27{,}670\ cm^{-1}$$

$$= 14{,}690\ cm^{-1},$$

which is a lower limit to $D_o'$ because the binding energy of the ground state has been assumed to be negligible.

It can also be seen from Figure 19 that the dissociation energy of the upper state can be calculated from the energy

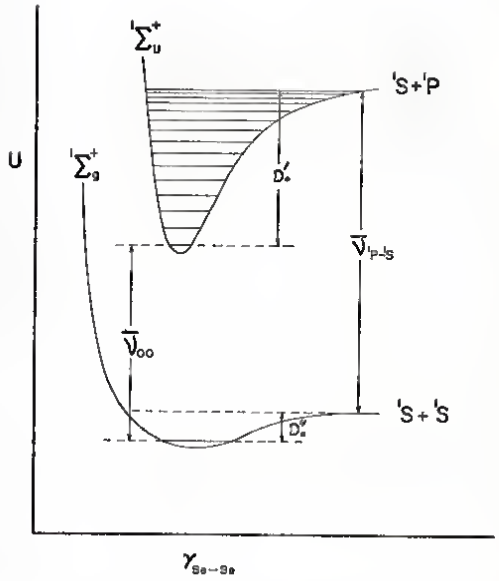


Figure 19. A schematic diagram of the potential energy curves for low lying states of the $Se_2$ molecule.

separations of its vibrational levels. Namely,

$$D_o = (G_{3/2} - G_{1/2}) + (G_{5/2} - G_{3/2}) + \ldots$$

or

$$D_o = \sum_{v'} \Delta G_{v'+1/2},$$

where $G_{v'+1/2}$ is the vibrational energy of the v' vibrational level of the state. For systems in which all of the v' transitions are observed up to the continuum, it is a simple matter to write down a list of transitions similar to Table 2 or 3 and to calculate $D_o'$ by adding up all the energy differences between adjacent absorption bands. For the many systems in which transitions are not observed up to the convergence point it is necessary to make an extrapolation to that point. A linear extrapolation was suggested by Birge and Sponer [18] which involves a plot of $\Delta G_{v'+1/2}$ versus v' with a linear extrapolation from the highest observed v' levels until the curve intersects the v' axis. The sum of the vibrational quanta in the electronic state is given very closely by the area under the $\Delta G$ curve. In most cases, however, $\Delta G$ is not a simple linear function of v' but possesses a downward curvature at higher v' values. So, the resulting extrapolated $D_o'$ values tend to be upper limits to the true $D_o'$ quantities. The areas under such extrapolated curves are usually some 25 to 30 percent greater than those beneath actual curves [19], and extrapolated dissociation energies are often too high by this amount.

Figure 20 shows an application of the linear Birge-Sponer extrapolation to the $^1\Sigma_u^+$ excited state of $Be_2$. The data points are taken from Table 3 and are the vibrational spacings of the upper state in an argon matrix. The area under curve (c) is the linearly extrapolated value of $D_o'$ and is calculated to be

$$D_o' = 1/2(48.6 \times 485\ cm^{-1}) = 11,800\ cm^{-1}\ .$$

Curve (b) represents a typical real plot of $\Delta G_{v'+1/2}$ versus v' showing negative curvature away from the linear extrapolation and having an enclosed area of about 9000 $cm^{-1}$. Curve (a) is as obtained by truncating the $\Delta G_{v'+1/2}$ series at the last observed absorption and gives a lower limit to $D_o'$ of 2716 $cm^{-1}$. When the data for $Be_2$ in neon matrices are treated similarly, the linear plot yields a value of 8800 $cm^{-1}$ for $D_o'$.

The values of $D_o'$ obtained from the Birge-Sponer plot are seen to be considerably lower than the values calculated previously from the atomic dissociation limit. A similar treatment of Brewer and Weng's $Mg_2$ data [7] yields $D_o' = 5100\ cm^{-1}$ compared with the value of 9311 $cm^{-1}$ determined from the gas phase spectrum by Balfour and Douglas [5]. It appears that the anharmonicity must be excessively large in the observed lower vibrational levels when these van der Waals molecules are trapped in matrices, so that one obtains low dissociation energies when the observed vibrational energy differences are linearly extrapolated to the dissociation limit.

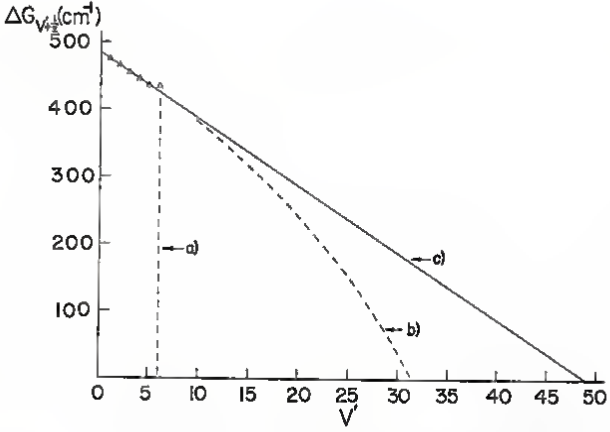
$\Delta G_{V+\frac{1}{2}}(cm^{-1})$
500
400
300
200
100
0
5
10
15
20
25
30
35
40
45
50
V'
a)
b)
c)

The high anharmonicity in the lower vibrational levels may be explained by the long-rang, attractive van der Waal's forces [10] of the atoms in the matrix cage for the atoms in the $Be_2$ molecule. This would explain the broadening of the potential curve at low values of v'. This explanation requires a compensatory steepening of the potential curve at higher values of v' for the trapped molecule to exhibit the required $^1P + {}^1S$ dissociation limit. Kaufman [20] has recently published a set of ab initio LCAO-MO-SCF calculations on the ground state interactions for the Be-Ne and Be-Ar systems. Although her results fail to detect a potential minimum for either system, both potential curves show sharp increases in repulsive energy at distances smaller than 7.0 Bohrs (3.7 Å) which could account for an increasing slope in the Be-Be potential at higher $r_{Be-Be}$ values.

Further support for this explanation is given by the work of Schnepp and Dressler [21,22] who studied the $^3\Sigma_u^- \leftarrow {}^3\Sigma_g^-$ transition of the oxygen molecule isolated in argon and nitrogen matrices. In both matrices the $^3\Sigma_u^-$ potential curve was found to be steeper for the perturbed oxygen molecule than for the free molecule at higher values of v'. A similar result was found by Brewer and Brabson [23], who studied the same transition of the $S_2$ molecule in nitrogen matrices.

The vibrational problem for diatomic molecules can be approximated by the well-known harmonic oscillator model, whose vibrational frequencies are given by the relation

$$\bar{\nu}c = (1/2\pi)(k/\mu)^{1/2}$$

where $\bar{\nu}$ is the vibrational energy in $cm^{-1}$, c is the speed of light ($3.0 \times 10^{10}$ cm/sec), k is the harmonic force constant, and $\mu$ is the reduced mass given for diatomic AB by

$$\mu = \frac{m_A \cdot m_B}{m_A + m_B} .$$

Solving for k gives

$$k = (c\bar{\nu})^2(2\pi)^2\mu$$

which yields k = 0.600 mdyne/Å for $Be_2$ in argon matrices. Harmonic force constants were also calculated for $Mg_2$ and $Ca_2$ using the gas phase data [5,6]. The results of these calculations appear in Table 5 which summarizes the $Be_2$ data and compares the spectroscopic results for $Be_2$ with the other known Group IIa diatomic molecules $Mg_2$ and $Ca_2$. It is apparent from the vibrational force constants for the ground and excited states that a stronger bond in the upper state arises from the promotion of an electron from a formally anti-bonding orbital in the ground state to a formally bonding higher energy orbital.

Using the harmonic force constant of 0.600 mdyne/Å for the $Be_2$ molecule, it is possible to calculate the Be-Be internuclear distance, in the excited state, $r_e$, by making use of the approximation known as "Badger's rule," [24,25] which states

$$k_e(r_e - d_{ij})^3 = C''$$

TABLE 5

$A^1\Sigma_u^+ \leftarrow X^1\Sigma_g^+$ TRANSITIONS OF GROUP IIA DIMER MOLECULES AND VIBRATIONAL FORCE CONSTANTS

| Molecule | $\nu_{00}(cm^{-1})$ | | $\Delta G'_{1/2}(cm^{-1})$ | | Vibrational Force Constants (mdyne/Å)[a] | |
|---|---|---|---|---|---|---|
| | Gas | Matrices | Gas | Matrices | $X^1\Sigma_g^+$ | $A^1\Sigma_u^+$ |
| $Be_2$ | --- | 28 551(Ne), 27 670(Ar) | --- | 489(Ne), 474(Ar) | --- | 0.600 |
| $Mg_2$ | 26 069[b] | 25 233(Kr), 24 522(Xe) | 190.6 | 199(Kr), 188(Xe) | 0.0185 | 0.257 |
| $Cs_2$ | 19 401[c] | 18 002(Kr)[d] | 130[c] | | 0.050 | 0.201[c] |

[a] 1 mdyne/Å = $10^{-5}$ dyne/cm = $10^{-8}$ N/m.

[b] Calculated from RKR potential curve fit to experimental data [5].

[c] Lowest v' transition observed.

[d] Tentative assignment [8].

where $d_{ij}$ is a constant that varies with the type of atoms in the molecule. If both atoms are in the first row of the periodic chart, $d_{ij}$ = 0.68 Å, and if both atoms are in the second row, $d_{ij}$ = 1.25 Å. C" may be taken as a constant for all molecules and is equal to 1.86 when $k_e$ is expressed in units of $10^5$ dynes/cm, and $d_{ij}$ in Å units ($10^{-8}$ cm). This approximation gives $r_e$ for $Be_2$ as 2.14 Å (4.04 Bohrs). Since the spectra indicate that $r_e$ for the A state is nearly equal to $r_e$ for the $X^1\Sigma_g^+$ state, then 2.14 Å is probably a good approximation to $r_e$ in the ground state of $Be_2$ also. This result compares favorably with Bender and Davidson's calculation [15], $r_e \cong 4.5$ Bohrs, where the potentials were computed at 0.5 Bohr intervals. Another check on Badger's approximation for $r_e$ was performed using the calculated force constant for $Mg_2$ (from Table 5). The resulting $r_e$ value was 3.18 Å, which is very close to the experimentally determined value of 3.082 Å [5]. Evidently this approximation works quite well even for molecular state having only 0.5 net bonds per molecule, such as the Group IIA metal dimers considered here.

## Summary

The $Be_2$ molecule has been observed for the first time by the technique of matrix isolation spectroscopy. A molecular progression assignable to the $A^1\Sigma_u^+ \leftarrow X^1\Sigma_g^+$ transition has shown the existence of a strongly bonding excited state

with $r_e$ = 2.14 Å and a vibretional force constant of 0.6 mdyne/Å. The obaarvation that $Be_2$ can be formed by annealing a matrix doped with Be atoms is in agreemant with diffusion experimanta with lithium in rare gas matrices [26] and demonetrates that thara is in fact a minimum in the potential energy curve for a pair of Be atoms.

Furthar work whith might be worthwhile for thia system would include a fluoreacence expariment in which a high intensity tuneabla light source could be centered on a particular vibrational band or group of banda while the matrix is eoanned for fluorescent emiseion at lower enargias in hopes of obaervieg vibrational atructure in transitions to tha loosaly bound ground state. In this way the depth of the attractive potential well in the ground state could ba measured.

Tha present expariments have also pointad to the need for new, more accurate ab initio calculations for the $Ba_2$ molecule. State-of-the-art calculations for this 8-electron molecula would help in tha assignment of the excited states and should prove to be theoratically rewarding in the study of van der Waals interactiona by providing a model which is amenabla to study both experimentally and theoretically.

REFERENCES, CHAPTER II


1. O.T. Nikitin and L.N. Gorokhov, Russ. J. Inorg. Chem. 6, 111 (1961).

2. W.A. Chupka, J. Berkowitz, and C.F. Giese, J. Chem. Phys. 30, 827 (1959).

3. D.L. Hildenbrand and L.F. Theard, J. Chem. Phys. 50, 5350 (1969).

4. R.H. Ewing and A.M. Mellor, J. Chem. Phys. 53, 2983 (1970).

5. W.J. Balfour and A.E. Douglas, Can. J. Phys. 48, 901 (1970).

6. W.J. Balfour and R.F. Whitlock, Chem. Comm., 1971, 1231 (1971).

7. L. Brewer and J. Wang, J. Mol. Spectry. 40, 95 (1971).

8. J.B. Francis, Jr. and S.E. Webber, J. Chem. Phys. 56, 5879 (1972).

9. P.H. Kasai, E.B. Whipple and W. Weltner, Jr., J. Chem. Phys. 42, 4055 (1965).

10. L.N. Shabanova, Optika i Spektroskopii 27, (3), 383 (1969).

11. W.H. Furry and J.H. Bartlett, Jr., Phys. Rev. 38, 1615 (1931).

12. B.J. Ransil, Rev. Mod. Phys. 32, 245 (1960).

13. B.J. Ransil and S. Fraga, J. Chem. Phys. 35, 669 (1961).

14. B.J. Ransil and S. Fraga, J. Chem. Phys. 36, 1127 (1962).

15. C.F. Bender and E.R. Davidson, J. Chem. Phys. 47, 4972 (1967).

16. E.R. Davidson, private communication.

17. M.A. Marchetti and S.R. LaPaglia, J. Chem. Phys. 48, 434 (1968).

18. R.T. Birge and H. Sponer, Phys. Rev. 28, 259 (1926).

19. G.W. King, Spectroscopy and Molecular Structure, (Holt, Rinehart, and Winston, Inc., New York, 1964).

20. Joyce J. Kaufman, J. Chem. Phys. 58, 4880 (1972).

21. O Schnepp and K. Dressler, J. Chem. Phys. 42, 2482 (1964).

22. O. Schnepp, J. de Chim. Phys. 62, 189 (1966).

23. L. Brewer and G.D. Brabson, J. Chem. Phys. 44, 3274 (1965).

24. R.M. Badger, J. Chem. Phys. 2, 128 (1934).

25. R.M. Badger, J. Chem. Phys. 3, 710 (1935).

26. L. Andrews and G.C. Pimentel, J. Chem. Phys. 47, 2905 (1967).

CHAPTER III

# SPECTROSCOPY OF MOLYBDENUM AND MOLYBDENUM OXIDES IN RARE GAS MATRICES

## Introduction

The study of the reactivity of metals at high temperatures in oxidizing atmospheres is especially important to the science of materials research and development, and of particular interest are the properties of the so-called refractory metals Nb, Mo, Ta and W which have melting points above 2400°C and are the most useful metals for high temperature service. These metals have the property that at high temperatures they form volatile oxides which have widely varying melting points. Table 6 contains a summary of the melting points and boiling points of these refractory metals and the melting points of their most commonly formed oxides along with the temperatures at which oxide volatility is first observed and at which complete volatility is observed. Gulbransen [1] has shown that the temperature for complete volatilization of the oxide and the melting point of the oxide determine the nature of the oxidation processes for these materials, low melting point and high volatility for the oxide indicating poor resistance to oxidation for the metal.

In order to characterize a refractory metal oxide system, the structural and energetic properties of the initial and

TABLE 6

PHYSICAL PROPERTIES OF THE REFRACTORY METALS AND THEIR OXIDES

Data from Gulbransen [1]

| Metal | Metal | | Metal Oxide | | Temperature (°C) at which oxide volatility is first observed | Temperature (°C) for complete volatilization of metal oxide |
|---|---|---|---|---|---|---|
| | M.P.°C | B.P.°C | Formula | M.P.°C | | |
| Nb | 2468 | 4759 | $Nb_2O_5$ | 1512 | N.D.[a] | N.D. |
| Mo | 2617 | 4692 | $MoO_3$ | 797 | >475 | >700 |
| Ta | 2997 | 5433 | $Ta_2O_5$ | 1877 | N.D. | N.D. |
| W | 3377 | 5618 | $WO_3$ | 1472 | >875 | >1250 |

[a] N.D. = not determined.

final states of the system are necessary, as well as the energies of all phase and structural modifications along with the physical conditions (T and P) needed to bring them about. Obviously a considerable overlap between the fields of high temperature thermodynamics, molecular spectroscopy, and chemical kinetics is necessary to describe such a system, and in no case has it been done completely. The spectroscopic parameters of these metal oxide molecules have frequently been determined by the matrix isolation technique because of the relative simplicity of the spectra in rare gas solids near 4°K compared to gas phase emission and absorption spectra.

The refractory metal-oxygen systems which have previously been thoroughly examined in rare gas matrices are W-$O_2$ [2], Nb-$O_2$ [3], and Ta-$O_2$ [4]. In each case, spectra assignable to the monoxide were observed as well as transitions which were due to higher oxides of the metal. The conspicuous absence of molybdenum from the list given above led to this investigation of the Mo-$O_2$ system, where it was expected that the observations might be quite similar to those for the W-$O_2$ system because of the vertical relationship between the metals in the periodic table.

Historically, the first band spectra assigned to MoO were observed by Piccardi [5] in an arc between silver electrodes sprinkled with powdered Mo and $MoO_3$. He tentatively assigned the weak bands in the region 610-650 nm to MoO because they were not observed in sources with temperatures below 2500°K. Piccardi also saw a continuum emission between

480 and 660 nm when Mo compounds were vaporized in an oxyacetylene flame. The continuum showed maxima at 630 and 522 nm and was assigned by Piccardi to either $MoO_3$ or a predissociation of MoO.

Swaminathan and Krishnamurthy [6] reported "as many as" 10 band systems when a DC arc was struck in air between Mo rods with $\omega_e'' = 940\text{-}960\ cm^{-1}$ in the same region as those bands observed by Piccardi. The details of the band analysis were never published, however, and the reported spectral features do not agree with the other published work for the Mo-$O_2$ system.

The atlas of Gatterer, Junkes, and Salpeter [7] lists 16 band heads assigned to MoO in the region 576-880 nm. Howard and Conway [8] using a plasma jet source proved by isotopic substitution with $^{15}N$ that 11 of the 16 bands assigned to MoO by Gatterer et al. were due to molecules of the empirical formula $Mo_xN$. The remaining near infrared "MoO Bands" have not been assigned to specific structural formulas but are definitely due to oxides of Mo along with bands at 650.9 and 644.5 nm, according to Howard and Conway [8].

Fortunately, the body of available spectral data in the infrared region is in better shape than that in the ultraviolet and visible portions of the spectrum. The gas phase infrared spectrum of the vapors over solid $MoO_3$ at high temperatures has been reported by Iorns and Stafford [9] to exhibit absorption features at 969 and 815 $cm^{-1}$ which they assigned to the Mo-O stretching and Mo-O-Mo ring vibrations of $(MoO_3)_3$,

respectively. Nikitin and Mal'tsev [10] in a similar experiment reported bands at 970 and 815 $cm^{-1}$ over $MoO_{3(s)}$ and also observed a band at 950 $cm^{-1}$ over hot $MoO_{2(s)}$ which they assigned to the antisymmetric vibration ($\nu_3$) of $MoO_2$.

Following up on his gas phase results, Mal'tsev et al. [11] obtained in an argon matrix the infrared absorption spectrum of the vapors produced when $MoO_3$(s) was heated to 660°C. The matrix showed absorptions at 977, 865, 856, and 837 $cm^{-1}$ in the region 400-1200 $cm^{-1}$. The 977 $cm^{-1}$ absorption was assigned to the out of plane Mo-O vibrations of rings of $MoO_3$ units with the remaining bands attributed to the ring vibrations of $(MoO_3)_5$, $(MoO_3)_4$, and $(MoO_3)_3$, respectively.

Single crystal raman spectra have been recorded for $MoO_3$ by Krasser [12], who assigned the 996 $cm^{-1}$ feature to the Mo=O stretch and the band at 826 $cm^{-1}$ to a vibration of the Mo-O-Mo bridge. His results were consistent with a crystalline model for $MoO_3$ having each Mo atom surrounded by a distorted octahedron of oxygen atoms as determined by x-ray diffraction [13].

Previous studies of Mo atoms isolated in rare gas matrices [14,15] have shown that the strong atomic transitions which are observed can be correlated with gas phase transitions from the $a^7S$ state to the $z^7P$ and $y^7P$ states. This background information is helpful in the analysis of the observed ultraviolet spectra in this work.

Most important to the assignment of the observed vibrational spectra in all of the experiments on the Mo-$O_2$ systems is the mass spectrometric work on the vaporization of the

different molybdenum oxides and the high temperature, low pressure reactions of Mo with $O_2$. The mass spectrum of the vapor over $MoO_3$ [16] showed the most abundant species to be $Mo_3O_9$, $Mo_4O_{12}$, and $Mo_5O_{15}$ with relative intensities ratios of 1.0:0.33:0.05, respectively, at a temperature of 850°K. The vaporization of solid $MoO_2$ [17] has been shown to produce $MoO_3$ as the most abundant gas phase molecule, followed in abundance by $(MoO_3)_2$, $MoO_2$, and $(MoO_3)_3$ over a range of temperatures from 1470-1785°K. When a stream of molecular oxygen is passed over the surface of hot Mo metal the major products which are formed are $MoO_2$ and $MoO_3$ [18] with the relative abundances changing with the temperature of the metal surface and with the oxygen pressure. The only reported mass-spectrometric observation of MoO [19,20] came from experiments in which Mo metal was heated in an $Al_2O_3$ crucible to temperatures above 2170°K, where the Mo oxides were found in order of abundance $MoO_2$ > MoO > $MoO_3$. This system, however, is not suitable for matrix isolation work because the pressures of Al, O, $Al_2O$, and AlO are 1 to 3 orders of magnitude greater than those of the oxides of molybdenum under these conditions.

## Experimental

The dewar used in this work has been previously described [21]. The matrices were formed on calcium fluoride or cesium iodide targets cooled to about 4°K with liquid helium. The outer windows of the dewar were of the same material as the

targets which were chosen according to the spectral region of interest for the particular experiment. The background pressure in the dewar was typically $2 \times 10^{-7}$ torr before filling with He and $4 \times 10^{-8}$ torr after filling.

Research grade argon was purchased from Matheson, and ultra-pure neon was obtained from Airco. The two rare gases were used without further purification other than passage through a copper coil immersed in liquid nitrogen to freeze out any condensable impurities. The molybdenum metal (99.9+%) was purchased from General Electric. High purity oxygen (99.998%) was purchased from Airco, and 91 percent enriched $^{18}O_2$ was purchased from Miles Yeda Laboratories to be used for isotopic substitution.

The molybdenum oxides were produced in the apparatus shown in Figure 21. The molybdenum cells were made from 1/8 inch o.d. tubing with a wall thickness of 0.020 inch and were cut to a nominal length of 1 inch on a Pistorius wheel with a carborundum disc. The ends of the cells were ground to a slight taper to assure a tight fit into the holes in the Mo rods which served as the endcaps and electrical contacts for the cells. These rods were shrink fitted into holes in the copper blocks to give good thermal and electrical connections and to prevent $O_2$ leakage. One of the Mo supports was drilled out and used as the $O_2$ inlet to the hot cell. The $O_2$ gas was leaked into one end of the Mo cell from a 30 cubic foot cylinder at 2000 psig. An oil free regulator was used to step the pressure down to about 2 psig and a needle valve

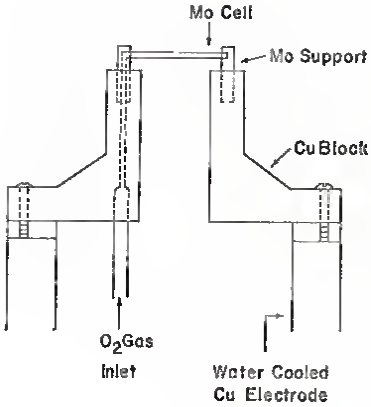


Figure 21. Apparatus for the production of Mo oxides.

was used to control the flow rate of gas through the cell. Under operating conditions the cells were typically heated to temperatures between 1700 and 2300°C, and the $O_2$ flow was controlled so that the pressure inside the furnace chamber could be varied from $2 \times 10^{-6}$ torr to $5 \times 10^{-5}$ torr with a typical background pressure being $2 \times 10^{-6}$ torr with the cell at 2200°C.

The cells were resistively heated by passing currents of several hundred amperes through them, and the surface temperature was monitored with a Leeds and Northrup optical pyrometer. All temperatures reported in this paper have been corrected for the nonideality of molybdenum as a black body emitter using the data of Worthing [22] as reported in the book by Espe [23] and are probably within 25° of the true temperature of the cell.

Experiments were also performed in which solid $MoO_3$ (Spex Industries, 99.99+%) was vaporized from a tantalum cell at temperatures ranging from 600-800°C with the products trapped in Ar and Ne matrices. The cell temperature was monitored with a chromel versus alumel thermocouple which was strapped to the hot cell with tantalum wire. The thermocouple output was measured using a Leeds and Northrup volt potentiometer. These experiments were done to confirm the Ar matrix results of Mal'tsev et al. [11] and to obtain higher resolution infrared spectra of the matrices than those reported in the previous work [11].

Absorption spectra were recorded from 1200 nm to 199

nm using a Jarrell Ash 0.5 meter Ebert mount monochromator. Gratings blazed at 300, 500, 800, and 1000 nm were used to span the spectral regions of interest. A tungsten ribbon lamp was used as the light source from 1200 to 350 nm and a Sylvania DE350 $D_2$ lamp was the source in the ultraviolet region. The detectors for this work were an RCA 7102 photomultiplier tube for the near infrared region and an RCA 7200 PMT for the visible and ultraviolet regions. Their outputs were fed into a Jarrell Ash electrometer amplifier and then recorded on a Bristol model 570 strip chart recorder. The visible and ultraviolet spectra were calibrated using a low pressure mercury arc lamp and measured to the nearest 0.5 nm unless otherwise noted.

Absorption spectra in the infrared were taken using a Perkin-Elmer 621 grating spectrophotometer and were routinely scanned from 4000-200 $cm^{-1}$. The double-beam spectra were recorded versus a nitrogen purged cell with two CsI windows which was positioned in the reference beam. This cell was equipped with an adjustable iris which allowed the operator to attenuate the reference beam to compensate for light scattered from the sample beam by the thicker matrices. The spectra were calibrated with the absorption spectrum of a thin film of polystyrene, and are accurately reported within a range of $\pm$ 0.5 $cm^{-1}$. The relative positions of bands could be measured and experimentally reproduced with an accuracy of $\pm$ 0.05 $cm^{-1}$ when the higher scale expansions were used.

## Observations

### Ultraviolet and Visible Spectra

Absorption features in argon matrices.--The absorption spectra of the argon matrices formed in this work were recorded over the range 800-245 nm. The most prominent bands in these matrices were absorptions assignable to Mo atoms. The spectra of Mo atoms isolated in Ar matrices have been reported by Schoch and Kay [14] and by Green and Gruen [15]. These authors agree on the assignment of all of the strong features which were seen, but their interpretations vary for some of the weaker bands. A summary of the absorption features in argon matrices recorded in this work is given in Table 7. Green and Gruen have suggested that some of the weaker absorptions which they observed in argon matrices are due to Mo dimers [15] or higher polymers and have substantiated these assignments with variable temperature experiments, showing that those features "grow in" as the matrix is warmed to a temperature where significant diffusion can occur. The bands which exhibited this behavior were found in two areas: (1) a broad absorption system at 517.5 nm and (2) several poorly resolved features at 310.7, 308.5, and 304.7 nm which appear between the intense absorptions assigned to the allowed atomic transitions. Similar absorption systems were discovered in Kr matrices where the ultraviolet system appeared as a progression of 3 bands with a vibrational spacing of about 340 $cm^{-1}$.

The spectra reported here for Mo in solid Ar do not show

TABLE 7

ULTRAVIOLET AND VISIBLE SPECTRA IN ARGON MATRICES

| $\lambda_{Ar}$(nm) | $\bar{\nu}_{Ar}$($cm^{-1}$) | $\bar{\nu}_{gas}$($cm^{-1}$) [24] | $\bar{\nu}_{Ar}-\bar{\nu}_{gas}$ | Upper State Assignment | | |
|---|---|---|---|---|---|---|
| | | | | Green and Gruen [15] | Schoch and Kay [14] | This Work |
| 765.1 | 13 067 | | | N.O.[a] | N.O. | oxide |
| 742.1 | 13 472 | | | N.O. | N.O. | oxide |
| 690.1 | 14 489 | | | N.O. | N.O. | oxide |
| 408.1 | 24 497 | | | N.O. | N.O. | oxide |
| 394.1 | 25 367 | | | N.O. | N.O. | oxide |
| 379.7 | 26 329 | | | N.O. | N.O. | oxide |
| 375.1 | 26 652 | | | N.A.[b] | N.A. | N.A. |
| 357.1 | 27 995 | 25 614 | 2 381 | $z^7P_2$ | $z^7P_2$ | $z^7P_2$ |
| 349.9 | 28 571 | 25 872 | 2 699 | $z^7P_3$ | $z^7P_3$ | $z^7P_3$ |
| 341.5 | 29 274 | 26 321 | 2 953 | $z^7P_4$ | $z^7P_4$ | $z^7P_4$ |
| 331.8 | 30 130 | | | N.O. | N.A. | oxide |
| 323.3 | 30 922 | 28 667 | 2 255 | N.O. | $z^7F_2$ | oxide |
| 288.0 | 34 712 | | | $y^7P_4$ | $y^7P_4$[c] | $y^7P_4$ |

TABLE 7 (continued

| $\lambda_{Ar}$(nm) | $\bar{\nu}_{Ar}$($cm^{-1}$) | $\bar{\nu}_{ges}$($cm^{-1}$) [24] | $\bar{\nu}_{Ar}-\bar{\nu}_{ges}$ | Upper State Assignment | | |
|---|---|---|---|---|---|---|
| | | | | Green and Gruen [15] | Schoch and Key [14] | This Work |
| 281.5 | 35 513 | | | O.R.[d] | N.O. | oxide |
| 267.2 | 37 414 | 35 169 | 2 245 | O.R. | $z^5F_4$ | oxide |

[a] N.O. = not observed

[b] N.A. = observed but not assigned.

[c] In Table V of ref. 14, this is misprinted as $y^7D_4$.

[d] O.R. = out of spectral region examined.

the polymer bands assigned by Green and Gruen, but in matrices which absorbed strongly in the metal-oxide stretching region in the infrared (discussed in a separate section), absorption features were observed which are assignable as transitions of molybdenum oxides. Figure 22 shows a comparison of two spectra, one having strong Mo atom absorptions with very weak bands in the IR, the other having strong Mo atom bands and strong IR absorptions in the Mo-O stretching region. The bands assigned to molybdenum oxides have also been seen in matrices formed from low temperature reactions in which the Mo atom absorptions were very weak.

Of the absorptions listed in Table 7 as oxide bands, those at wavelengths longer than 390 nm were all extremely weak, often showing a change in transmittance of 1 percent or less from the continuum background radiation of the source. The bands were assigned on the basis of a careful comparison of a number of different spectra from several different experiments, and only those features which were reproducible are listed.

When matrices were formed by trapping the vapors over hot $MoO_3$(s) in Ar, absorption bands were detected in the near infrared region at 1134, 1129, and 1125 nm (8816, 8855, and 8886 $cm^{-1}$) as shown in Figure 23, but no absorptions were noted in the visible or ultraviolet regions down to 245 nm. These absorptions are probably assignable to polymers of $MoO_3$ which are the most abundant species over the solid in the temperature range 600-800°C [16].

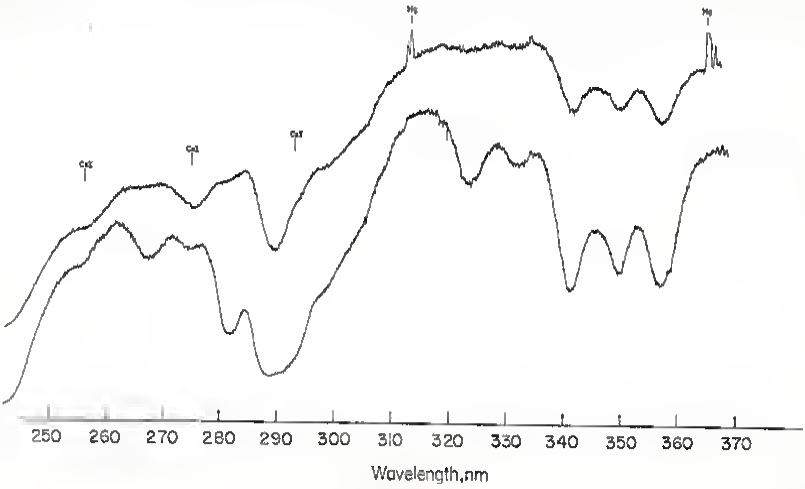


Figure 22. Ultraviolet absorption spectra of Mo atoms and Mo oxides in Ar matrices. The upper spectrum was recorded for a matrix having a moderate Mo atom concentration and a low Mo oxide concentration. The lower spectrum is for a matrix containing Mo atoms and a high Mo oxide concentration.

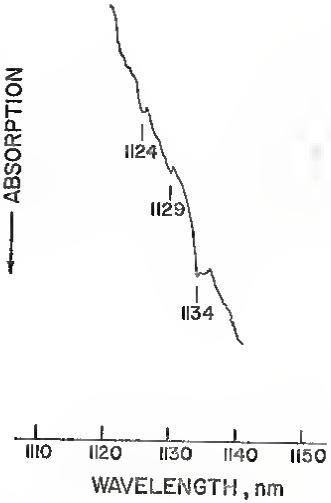


Figure 23. Near infrared absorption spectrum of species vaporized from hot $MoO_3$(s) and trapped in an Ar matrix.

Absorption features in neon matrices.--The absorption spectra of the neon matrices were recorded over the range 800-245 nm with the exception of one experiment in which the CsI target and windows were replaced with $CaF_2$ optics where the ultraviolet range was extended to 190 nm. When samples were deposited with the Mo cell at temperatures above 2000°C, the strongest absorptions which were seen were assignable as Mo atomic transitions. Figure 24 shows the ultraviolet spectrum of a matrix deposited from a Mo cell at 2125°C. The prominent features are the strong triplet at about 305 nm and the single band at 359.3 nm. The features at 303.0, 305.5, and 307.4 nm are attributed to the transitions from the atomic ground state $(Ar)4d^5 5s\ ^7S_3$ to the excited levels $y^7P_4$, $y^7P_3$, and $y^7P_2$, respectively. The lone band at 359.3 nm is the third member of the triplet shown in Figure 25. These absorptions occur at 371.5, 366.5, and 359.2 nm and are assigned as transitions to the $z^7P_2$, $z^7P_3$, and $z^7P_4$ atomic states, in that order.

Neon matrices which had infrared absorptions in the Mo-oxygen stretching region (1000-800 $cm^{-1}$) also exhibited a variety of absorption features in the ultraviolet region of the spectrum. The bands attributed to molybdenum oxides were extremely weak absorbers in the UV-visible region as was the case in argon, and the multitude of different oxides which is formed (via infrared analysis) precludes the assignment of these feeble absorptions to specific oxides of Mo. The only strong oxide bands which were observed were found in the

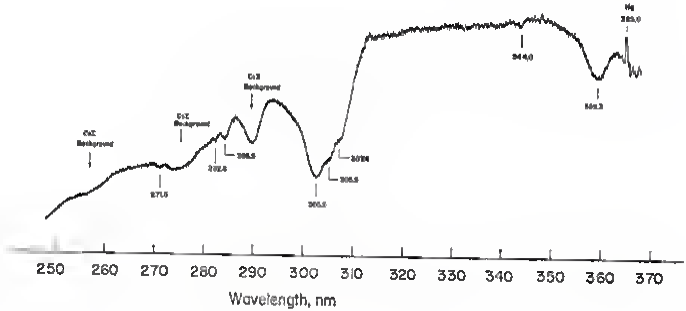


Figure 24. Ultraviolet spectrum of a Ne matrix containing Mo atoms and Mo oxides.

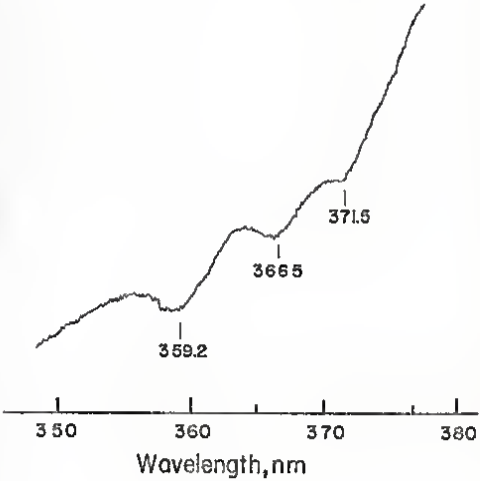


Figure 25. $z^7P \leftarrow a^7S$ absorption of Mo atoms in a Ne matrix.

far UV at 212.0 and 229.7 nm with a shoulder at 243.7 nm (see Figures 26 and 27). Unfortunately it was impossible to observe these bands in the same experiments as those in which the infrared spectra were recorded because of the infrared cutoff frequency of the $CaF_2$ optics, but in similar experiments the most abundant oxides which were formed were $MoO_3$ and its polymers. A summary of the atomic and oxide absorption bands in neon matrices is given in Table 8.

The absorptions at 344.0 and 271.5 nm, although very weak, were reproducible and were assigned to Mo oxides. The feature at 282.6 nm was assigned as the atomic transition to the $y^5P_3$ state on the basis of its gas to matrix frequency shift and its constant intensity relative to the other Mo atom absorptions in different experiments. This absorption was obscured in the Ar matrices by the CsI background absorption. The band listed in Table 8 at 322.9 nm does not appear in Figure 24, but was observed in matrices formed from lower temperature deposits (T < 1800°C) in which the Mo atomic absorptions were not observed.

Several neon matrices with high Mo atom concentrations were formed, and the resulting absorption spectra revealed a band system between the $y^7P$ and $z^7P$ atomic systems which appears to be due to Mo dimers or higher polymers formed in the matrix (see Figure 28). In the same matrices a strong absorption system was noted in the neighborhood of 510 nm (see Figure 29) which also appears to belong to polymeric Mo species. These bands, which were only seen in matrices having

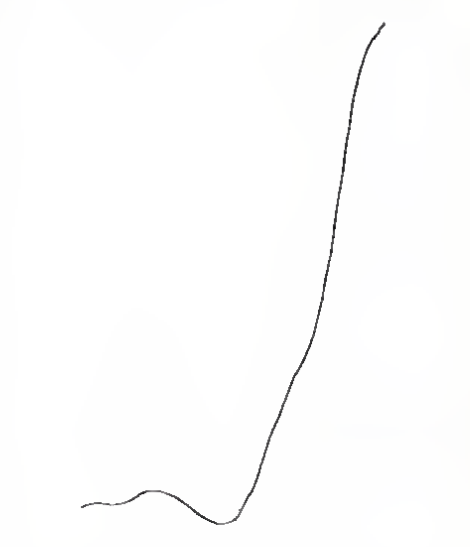


Figure 26. Far ultraviolet absorption spectrum of a Ne matrix containing Mo oxides. The absorption peaks are at 212.0, 229.5, and 243 nm.

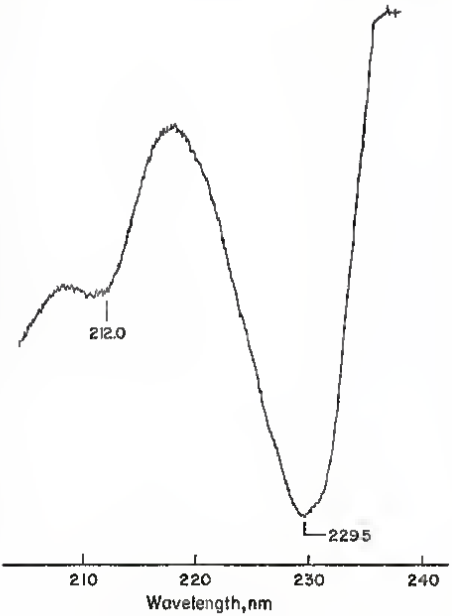


Figure 27. Far ultraviolet absorption spectrum of a Ne matrix containing Mo oxides--expanded scale.

TABLE 8

ULTRAVIOLET ABSORPTIONS IN NEON MATRICES

| $\lambda_{Ne}$ (nm) | $\bar{\nu}_{Ne}$ ($cm^{-1}$) | $\bar{\nu}_{gas}$ ($cm^{-1}$) [24] | $\bar{\nu}_{Ne}-\bar{\nu}_{gas}$ | Assignment |
|---|---|---|---|---|
| 371.5 | 26 910 | 25 614 | 1 296 | $z^7P_2$ |
| 366.5 | 27 277 | 25 872 | 1 405 | $z^7P_3$ |
| 359.2 | 27 831 | 26 321 | 1 510 | $z^7P_4$ |
| 344.0 | 29 061 | | | oxide |
| 332.9 | 30 030 | | | oxide |
| 307.4 | 32 521 | 31 300 | 1 221 | $y^7P_2$ |
| 305.5 | 32 723 | 31 533 | 1 190 | $y^7P_3$ |
| 303.0 | 32 994 | 31 913 | 1 081 | $y^7P_4$ |
| 284.5 | 35 139 | | | oxide |
| 282.6 | 35 375 | 33 955 | 1 420 | $y^5P_3$ |
| 271.5 | 36 822 | | | oxide |
| 243.7 | 41 022 | | | oxide (shoulder) |
| 229.7 | 43 522 | | | oxide |
| 212.0 | 47 154 | | | oxide |

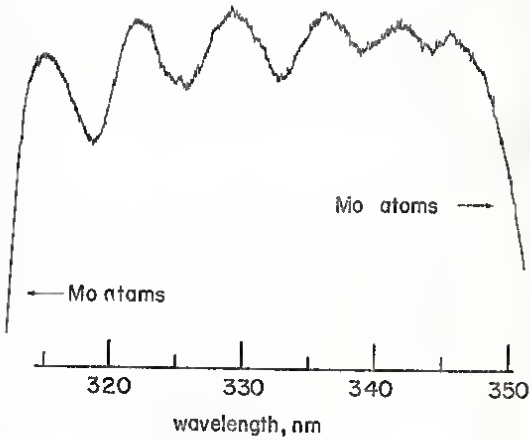


Figure 28. Mo polymer absorption (possible $Mo_2$) in a Ne matrix. The strong bands at each end of the figure are the Mo atomic absorptions shown in Figure 23.

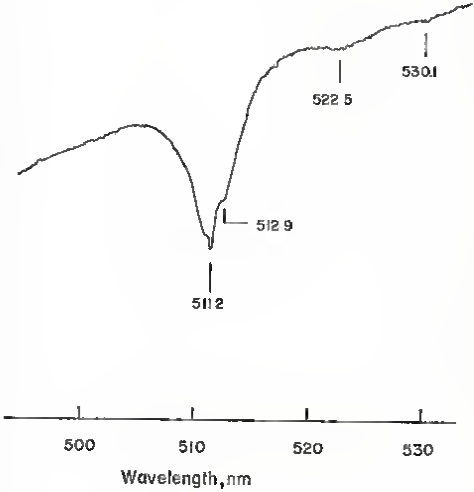


Figure 29. Mo polymer absorption in a Ne matrix.

a high concentration of Mo atoms, are analogous to absorptions reported by Green and Gruen [15] in annealed Ar and Kr matrices, of which the ultraviolet bands were tentatively assigned as Mo dimers with $\Delta G' = 340\ cm^{-1}$ in the excited state in the Kr matrix. The bands recorded in this work in solid Ne appear to show a more well-defined vibrational progression than the 3 observed bands in Kr, but the larger value of $\Delta G'$ and the variation in spacing between adjacent bands (see Table 9) cast some doubt on the assignment of these peaks as dimers, and it is possible that they are not assignable to the same absorbing species as those bands reported by Green and Gruen [15] but may be due to several different polymeric Mo species.

A comparison of the $z^7P \leftarrow a^7S$ atomic transitions in Ne with the previously published spectra in Xe, Kr, and Ar [15] reveals an anomalous frequency shift for the Ne spectra with respect to the other matrix spectra. Although the signs and magnitudes of the frequency shifts relative to the gas phase are difficult to predict, it is usually found for the series of rare gases that the transition energies for a particular atomic solute fall in the order Ne > Ar > Kr > Xe as predicted by the Lennard-Jones potential model put forth by Robinson [25]. However, in the case of Mo atoms it was observed that the Mo transition energies in the series of rare gases appeared in the order Ar > Kr > Ne > Xe > gas. A similar phenomenon was noted by Brewer, Meyer, and Brabson [26] in their study of Hg atoms, where the Ne transition energies were observed to

TABLE 9

ABSORPTIONS OF Mo POLYMERS IN NEON MATRICES

A. Bands Tentatively Assigned to $(Mo)_2$

| $(v',v'')$ | $\lambda$(nm) | $\bar{\nu}(cm^{-1})$ | $\Delta G'(cm^{-1})$ |
|---|---|---|---|
| $(v'_o,0)$[a] | 343.7 ± 0.3 | 29 087 ± 26 | |
| | | | 473 |
| $(v'_o+1,0)$ | 338.3 ± 0.3 | 29 560 ± 26 | |
| | | | 525 |
| $(v'_o+2,0)$ | 332.3 ± 0.2 | 30 085 ± 17 | |
| | | | 704 |
| $(v'_o+3,0)$ | 324.7 ± 0.2 | 30 789 ± 18 | |
| | | | 839 |
| $(v'_o+4,0)$ | 318.1 ± 0.1 | 31 428 ± 9 | |

B. Other Polymer Absorptions

| $\lambda$(nm) | $\bar{\nu}(cm^{-1})$ |
|---|---|
| 511.2 ± 0.1 | 19 556 ± 4 |
| 512.9 ± 0.2 | 19 492 ± 8 |
| 522.5 ± 0.5 | 19 133 ± 19 |
| 530.1 ± 1.0 | 18 859 ± 35 |

[a] $v'_o$ is the vibrational quantum number assigned to the first observed level of the upper state.

lie between those for Ar and Kr matrices. That case was explained by the assumption that only in Ne matrices did the impurity atom fail to occupy a substitutional lattice site, thus invalidating the Robinson theory which assumes a 12 nearest neighbor lattice site for the impurity. Although more recent discussions have suggested that the trapping of an impurity atom in a substitutional site is a highly improbable occurrence [27], and that in fact most impurities are trapped in sites having one or more vacancies in the nearest neighbor shell [28,29], it does appear that there is a specific interaction in the Ne host, which is different in the other solid rare gases, that can shift the impurity transitions to lower energies than those predicted by the Robinson model. McCarty [30] has recently shown that the correlation of the gross shifts in the spectrum of Hg in solid rare gases is greatly improved when the distortion of the rare gas lattice by the solute particle is taken into account. The characterization and explanation of this phenomenon depend on the extension of Ne matrix isolation to a larger number of systems, many of which have been previously examined only in Ar and Kr matrices.

Of the absorption features which have been observed in the ultraviolet and visible regions, those strong absorptions assigned to Mo atomic transitions have been shown to correlate reasonably well with transitions from the $a^7S$ ground state observed in the gas phase [24] and in other rare gas matrices [14,15]. Those bands which have been assigned as Mo oxide

absorptions were, with the exception of those below 250 nm, extremely weak, even in matrices showing intense Mo oxide bands in the infrared; and since there are no identifiable or obvious vibrational progressions, identification of these bands, even as oxide molecules is very difficult. Therefore the assignments of these weak features to molybdenum oxides are very tentative.

Infrared Spectra

Depending on the specific vaporization conditions it should be possible to observe the infrared absorption spectra of all the molybdenum oxides which have been mentioned: MoO, $MoO_2$, $MoO_3$, $(MoO_3)_2$, $(MoO_3)_3$, $(MoO_3)_4$, and $(MoO_3)_5$. The vapor over $MoO_3$(s) should contain $(MoO_3)_3$, $(MoO_3)_4$, and $(MoO_3)_5$ as the principal species in decreasing order of abundance [16]. When $O_2$ is passed over a hot Mo surface the major products should be $MoO_2$ and $MoO_3$ [18], and if there is some solid $MoO_2$ present $(MoO_3)_2$ may also be formed [17].

Vaporization of $MoO_3$(s).--The infrared spectra of the matrix isolated products formed when $MoO_3$(s) was vaporized from a Ta cell at temperatures near 700°C are shown in Figures 30 and 31 for Ar and Ne matrices, respectively. The line positions in Ar and Ne are listed in Tables 10 and 11 along with the relative intensities and half widths of the absorption bands. It is immediately obvious that the neon spectra are sharper and exhibit more structure than the argon spectra. This effect was observed in all the experiments on Mo oxides reported in this work, and the main reason that Ne matrices were employed was that greater spectral resolution was obtainable

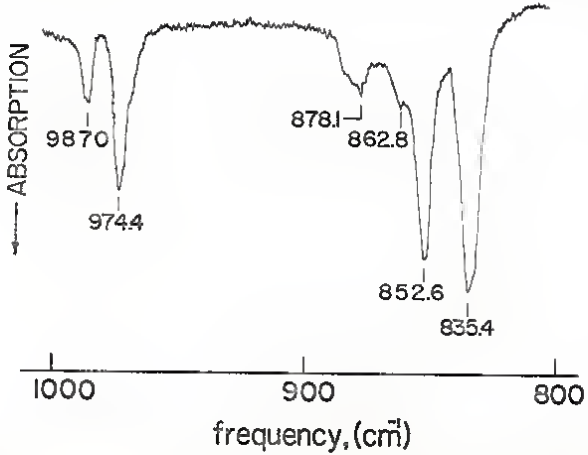


Figure 30. Infrared absorption spectrum of an Ar matrix containing species vaporized from hot $MoO_3$(s).

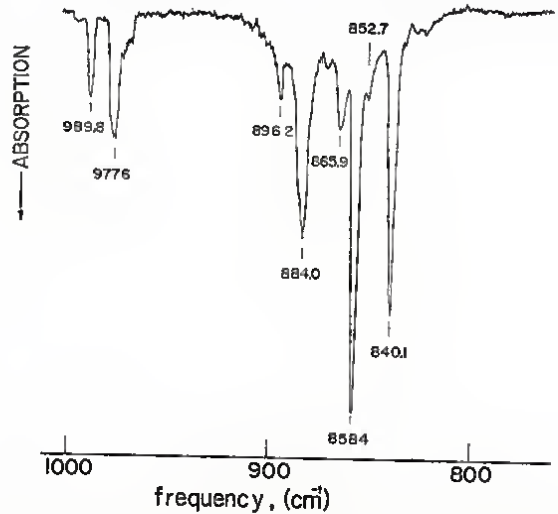


Figure 31. Infrared absorption spectrum of a Na matrix containing species vaporised from hot $MoO_3$(s).

TABLE 10

MAJOR INFRARED ABSORPTIONS OBSERVED FOR THE SPECIES VAPORIZED FROM HOT $MoO_3$(s) AND TRAPPED IN ARGON MATRICES

| $\tilde{\nu}$($cm^{-1}$) | Relative Intensity | Half Width ($cm^{-1}$) |
|---|---|---|
| 987.0 | 0.27 | 5.3 |
| 974.4 | 0.59 | 6.6 |
| 878.1 | 0.27 | 14.5 |
| 862.8 | shoulder | |
| 852.6 | 0.88 | 6.6 |
| 835.4 | 1.00 | 9.5 |
| 513.7 | 0.14 | 5.9 |

TABLE 11

MAJOR INFRARED ABSORPTIONS OBSERVED FOR THE SPECIES VAPORIZED FROM HOT $MoO_3$(s) AND TRAPPED IN NEON MATRICES

| $\bar{\nu}(cm^{-1})$ | Relative Intensity | Half Width ($cm^{-1}$) |
|---|---|---|
| 991.5 | shoulder | 2.6 |
| 989.8 | 0.21 | 5.3 |
| 977.6 | 0.31 | |
| 973.3 | shoulder | |
| 971.0 | shoulder | |
| 969.7 | shoulder | |
| 896.2 | 0.20 | 5.2 |
| 884.0 | 0.58 | 6.3 |
| 865.9 | 0.28 | 4.2 |
| 863.5 | shoulder | |
| 858.4 | 1.00 | 3.8 |
| 852.7 | shoulder | |
| 840.1 | 0.77 | 3.3 |
| 514.1 | 0.12 | 6.0 |

in them than in Ar.

The absorption spectra presented in Figures 30 and 31 must be interpreted as the convoluted spectra of the species known to be present in greatest quantities in the vapor over $MoO_3$(s), namely, $(MoO_3)_3$, $(MoO_3)_4$, and $(MoO_3)_5$ [16]. The trimer $(MoO_3)_3$ has been shown by electron diffraction to exist as a six-membered planar $Mo_3O_3$ ring ($D_{3h}$ symmetry) in which each Mo atom is also bound to a pair of O atoms outside the plane of the ring [31] (see Figure 32). Presumably the tetramer and pentamer have similar ring type structures also. It was on this basis that Mal'tsev et al. [11] attempted to explain their observed spectra in Ar matrices. Unfortunately they were unable to identify the peak at 878 $cm^{-1}$ because of a background absorption in their apparatus. Also notable is the absence of the absorptions at 987 and 514 $cm^{-1}$ from the spectra of Mal'tsev, since these bands were quite easily reproduced over the temperature range 600-800°C in this work, bracketing the source temperature of 660°C reported by Mal'tsev [11]. It was found, however, that as the rare gas flow was increased and the source temperature was increased (both of which should result in a decrease in the fraction of higher polymers, the former by reducing polymerization in the matrix and the latter by changing the composition of the vapors over the solid $MoO_3$) the intensities of the 987 $cm^{-1}$ and 878 $cm^{-1}$ absorptions in Ar matrices decreased a small but measurable amount relative to the other absorption features. This indicates the possibility that higher polymers of $MoO_3$ than the

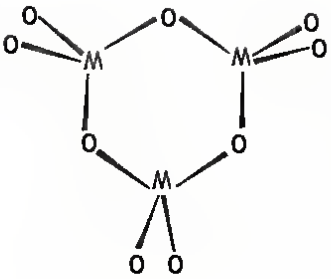


Figure 32. Ring structure of the metal oxide molecules $(MO_3)_3$, where M is Molybdenum or Tungsten.

pentamer, or structural units other than rings of $MoO_3$, may have been trapped in the matrix, and in fact the 987 $cm^{-1}$ absorption is very near the 989 $cm^{-1}$ vibrational frequency which is characteristic of crystalline $MoO_3$. This solid is known to exist as an array of Mo atoms, each surrounded by a distorted octahedral arrangement of 6 oxygen atoms [13].

The complexity of the neon spectra indicates that the vibrational transitions for these molecules are too numerous and complicated to be interpreted by the simple one-to-one peak assignments of Mal'tsev [11]. In Ar matrices the strong peak at 974.4 $cm^{-1}$ has been correlated with a gas phase absorption [9] at 969 $cm^{-1}$ and assigned as the stretching frequency for the out of plane Mo=O bonds in the trimer, tetramer, and pentamer. The neon spectra, however, indicate under higher resolution that there may be 4 or more different transitions in this region which occur at different frequencies, namely, 977.6, 973.3, 971.0, and 969.7 $cm^{-1}$. While it does seem reasonable to assign the two most intense bands in the region between 800 and 900 $cm^{-1}$ to the trimer and tetramer ring vibrations, the variation in the relative intensities of the absorption peaks on going from Ar to Ne matrices raises serious doubts concerning the assignment of either peak to a specific molecule. The Ar spectra would lead one to assign the low frequency member of the group to the trimer on an intensity basis, whereas in Ne the same argument would label the middle peak as the trimer vibration. Further work is needed to clarify the interpretation of the vibrational spectra for these large molecules.

Oxidation of Mo (1700-1850°C).--When $O_2$ gas was passed at low pressures through the apparatus shown in Figure 21 with the products being trapped in a rare gas matrix, the infrared absorptions of the resulting matrices could be seen to vary with the temperature of the Mo cell. Typical spectra obtained in Ne and Ar from Mo cells flushed with $^{16}O_2$ at 1725°C are shown in Figures 33 and 34. A comparison of all the infrared spectra observed in the experiments performed with this apparatus at temperatures ranging from 1700-2000°C revealed a group of three bands that always appeared simultaneously and in the same intensity ratios, indicating that they are probably assignable to the same molecular species. These bands were found in Ne at 975.7, 694.2, and 350.1 $cm^{-1}$. As the temperature of the Mo cell was increased and the oxygen flow decreased, it was observed that the relative intensities of these 3 bands were diminished in favor of other observed absorptions. None of the absorption features in this group revealed any fine structure under high resolution scans in either matrix, which suggests, along with the temperature dependence, that the three bands belong to a molecule containing more than one Mo atom, as explained below.

Natural Mo comprises 7 stable isotopes which are listed with their natural abundances and atomic masses in Table 12. Species containing two or more Mo atoms would probably not exhibit resolvable isotope structure because of the many possible, closely spaced combinations of these 7 isotopes, whereas those species containing a single Mo atom should be

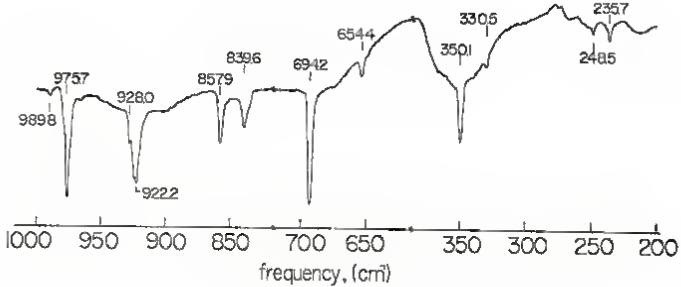


Figure 33. Infrared absorption spectrum of a Na matrix containing Mo oxides formed by passing $O_2$ gas through a Mo cell at 1725°C.

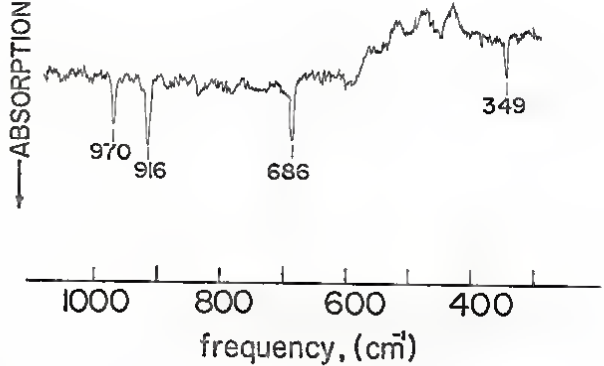


Figure 34. Infrared absorption spectrum of an Ar matrix containing Mo oxides formed by passing $O_2$ gas through a Mo cell at 1725°C.

TABLE 12

NATURAL OCCURRING STABLE ISOTOPES OF Mo

| Isotope | Percent Natural Abundance [32] | Atomic Mass (amu) [32] |
|---|---|---|
| $^{92}Mo$ | 15.64 | 91.9063 |
| $^{94}Mo$ | 9.04 | 93.9047 |
| $^{95}Mo$ | 15.72 | 94.9046 |
| $^{96}Mo$ | 16.53 | 95.9046 |
| $^{97}Mo$ | 9.46 | 96.9056 |
| $^{98}Mo$ | 23.78 | 97.9055 |
| $^{100}Mo$ | 9.13 | 99.9076 |

recognizable by their characteristic Mo isotope distributions.

The absorption band near 925 $cm^{-1}$ in Ne shows an extremely reproducible fine structure which is interpreted as being the normal Mo isotope structure rather than the frequently observed matrix splitting effect. This conclusion is based on the following reasons. First, the fine structure could be reproduced over a wide range of matrix concentrations and source temperatures; and second, the observed splitting pattern and intensity ratios agree with the known isotopic distribution in natural Mo.

A mass spectrometric investigation of the oxidation of Mo surfaces in this temperature range [18] has shown $MoO_3$ and $MoO_2$ to be the most important volatile oxides formed. However, in the presence of any solid oxide the distribution of volatile products is shifted in favor of the higher polymers, with the order of abundance being: $MoO_3 > (MoO_3)_2 > MoO_2 > (MoO_3)_3$ [17]. It was observed in the present work that at the ends of the Mo cells, where they were attached to the cooled Mo electrodes, some solid oxide could always be found. So, on the basis of these facts and the high temperature experiments reported in the next section, the structured absorption near 925 $cm^{-1}$ in Ne (915 $cm^{-1}$ in Ar) is assigned to the $MoO_3$ molecule. The group of 3 related absorptions mentioned above is tentatively attributed to the $(MoO_3)_2$ dimer on the basis of the above arguments and the fact that those frequencies were not observed in matrices known to contain the trimer, $(MoO_3)_3$, and higher polymers vaporized from $MoO_3$(s).

The presence of the absorptions at 858 and 840 $cm^{-1}$ in the Ne matrix which was formed at the lowest cell temperature and rare gas flow rate of this series of experiments yields another clue in the assignment of the vibrational frequencies of these metal oxide molecules. The two frequencies mentioned above were also noted in the matrices formed from the vaporization products of $MoO_3$(s), and the relative intensities ($I_{840}$:$I_{858}$) of these two bands are very nearly equal in the two very different experiments, namely, 0.77:1.00 in the vaporization from $MoO_3$(s) and 0.71:1.00 in the high temperature oxidation of the metal. These observations suggest that the assignment of the ring vibration frequencies at 840 and 858 $cm^{-1}$ along with an Mo=O stretch near 975 $cm^{-1}$ be made to the same polymeric species, probably $(MoO_3)_3$, which is the most abundant polymer, other than the dimer to be formed under the stated experimental conditions.

Frequently in this series of experiments absorption bands were recorded in the region of 200-300 $cm^{-1}$ (see Figures 33, 35 and 39, for example). The appearance of these features could not be positively correlated with any of the major absorptions in the stretching region. Most probably these low frequency bands are bending vibrations of polymeric species or possibly interionic vibrations of ion pairs trapped in the matrix, but assignments of these features to particular molecules are not warranted on the basis of the meager experimental details obtained in that spectral region.

Oxidation of Mo (1900-2200°C).--When the Mo cell was heated to temperatures in the neighborhood of 2100°C the absorption spectrum was observed to change once again as the distribution of volatile oxide products was shifted toward a mixture consisting of only the monomers, $MoO_2$ and $MoO_3$. By varying the cell temperature and oxygen flow it was possible to produce matrices with varying ratios of $MoO_2$: $MoO_3$. Typical spectra of deposits made from Mo cells at temperatures near 2100°C are shown in Figures 35 and 36 for Ar and Ne matrices. The new features which appear near 900 $cm^{-1}$ in Ne and 885 $cm^{-1}$ in Ar can be seen to exhibit a resolvable fine structure which is recognizable in the Ne spectrum as the Mo isotope structure mentioned previously. A high resolution scan of these features (see Figure 37) clearly reveals the Mo isotope pattern, indicating the presence of a single Mo atom in the molecule. The frequencies and isotopic splittings for these absorption systems are listed in Table 13. On the basis of the mass spectrum analysis referred to previously [18], the observed dependence of the absorption spectrum on the deposition temperature, and $^{18}O$ isotopic substitution results to be presented below, the new features near 900 $cm^{-1}$ and 885 $cm^{-1}$ in Ne and Ar are assigned to the $MoO_2$ molecule.

A more detailed analysis of these high temperature deposits reveals bands at 938.7 $cm^{-1}$ in Ar and 949.5 $cm^{-1}$ in Ne which appear in the entire series of high temperature deposits with constant intensity relative to the $MoO_2$ absorptions

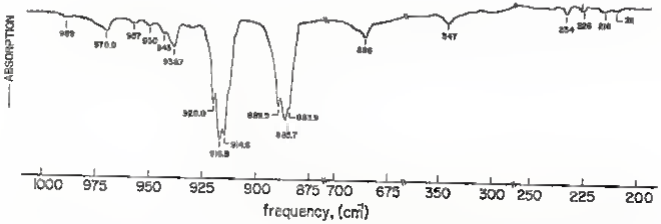


Figure 35. Infrared absorption spectrum of an Ar matrix containing Mo oxide formed by passing $O_2$ gas through a Mo cell at 2100°C.

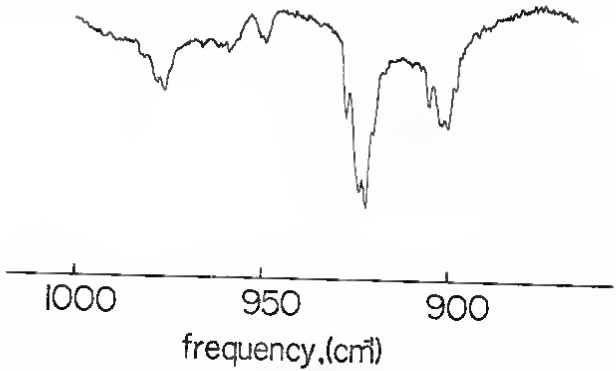


Figure 36. Infrared absorption spectrum of a Ne matrix containing Mo oxides formed by passing $O_2$ gas through a Mo cell at 2100°C.

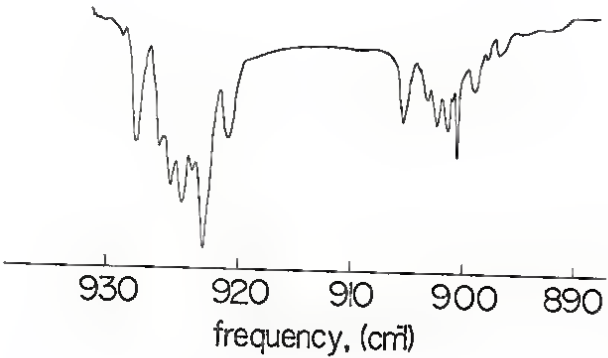


Figure 37. High resolution infrared absorption spectrum of a Ne matrix containing Mo oxides formed at high temperatures (2100°C) using $^{18}O_2$.

TABLE 13

ISOTOPIC FREQUENCIES FOR Mo OXIDES IN Ne MATRICES

| Molecule | Mo Isotope | $\nu(^{16}O)$[a] ($cm^{-1}$) | $\nu(^{18}O)$ ($cm^{-1}$) | $(\nu^{18}/\nu^{16})$ |
|---|---|---|---|---|
| $MoO_3$ | 92 | 982.2[b] | 937.42 | 0.9544 |
| | 94 | 980.0 | 936.42 | 0.9555 |
| | 95 | unresolved | 935.22 | |
| | 96 | 978.6 | 934.24 | 0.9547 |
| | 97 | unresolved | unresolved | |
| | 98 | 976.7 | 933.32 | 0.9556 |
| | 100 | 975.0 | 931.42 | 0.9553 |
| $MoO_3$ | 92 | 927.98 | 886.30 | 0.9551 |
| | 94 | 926.00 | 884.24 | 0.9549 |
| | 95 | 925.06 | 883.15 | 0.9547 |
| | 96 | 924.04 | 882.32 | 0.9548 |
| | 97 | 923.26 | unresolved | |
| | 98 | 922.17 | 880.34 | 0.9546 |
| | 100 | 920.33 | 878.52 | 0.9545 |
| $MoO_2$ | unresolved | 949.5[b] | 896.8[b] | 0.944 |

[a] Absolute error $\pm 0.5$ $cm^{-1}$; relative error $\pm 0.05$ $cm^{-1}$.

[b] Relative error $\pm 0.1$ $cm^{-1}$ for this system.

TABLE 13 (continued)

| Molecule | Mo Isotope | $\nu(^{16}O)^a(cm^{-1})$ | $\nu(^{18}O)(cm^{-1})$ | $(\nu^{18}/\nu^{16})$ |
|---|---|---|---|---|
| $MoO_2$ | 92 | 905.55 | 864.97 | 0.9552 |
| | 94 | 903.38 | 862.99 | 0.9553 |
| | 95 | 902.50 | 861.95 | 0.9551 |
| | 96 | 901.51 | 861.07 | 0.9551 |
| | 97 | 901.00 | 860.12 | 0.9546 |
| | 98 | 900.14 | 859.28 | 0.9546 |
| | 100 | 899.12 | 857.38 | 0.9536 |

previously mentioned. The structure of this molecule, assuming the Mo atom to be between the oxygens rather than a peroxide structure, must be either linear ($D_{\infty h}$ symmetry) or bent ($C_{2v}$ symmetry). If the molecule is linear the $\nu_1$ symmetric stretching vibration should not be infrared active, but for a bent $MoO_2$ the $\nu_1$ vibration should be seen and is expected to be weaker in intensity than the asymmetric stretch, $\nu_3$. Also, the $\nu_1$ vibration should show smaller Mo isotope splittings than $\nu_3$ due to the reduced motion of the Mo atom in this type of vibration, an effect which was observed for the bands mentioned above. On the basis of these arguments, the weak features at 938.7 and 949.6 $cm^{-1}$ in Ar and Ne, respectively, are assigned as the $\nu_1$ vibrations of a bent $MoO_2$ molecule with the stronger peaks near 885 and 900 $cm^{-1}$ shown in Figures 35 and 36 assigned to $\nu_3$, the asymmetric stretch.

Another observation which can be made in the high temperature deposits is the fact that there is a weak absorption feature showing the Mo isotope structure in Ne with the strongest peak at 976.1 $cm^{-1}$. This absorption appears to be associated with the $MoO_3$ system near 925 $cm^{-1}$ on the basis of relative intensity measurements in the absence of the other species which have shown absorptions in the 970 $cm^{-1}$ region, and is therefore attributed to the $MoO_3$ molecule.

Isotopic substitution with $^{18}O_2$.--In order to confirm that the absorption features which have been reported so far were, in fact, due to oxides of Mo and to assist in the characterization of these features, experiments were made

using 90 percent $^{18}O_2$ as the oxidizing gas instead of the usual $^{16}O_2$. A high resolution scan of the $^{18}O$ substituted monomer absorptions in Ne is shown in Figure 38. The frequencies and isotope shifts are listed in Table 13. These can be compared with the calculated ratio ($\nu^{18}/\nu^{16}$) for $^{98}MoO$ which is 0.9509 in the harmonic oscillator approximation, thus assuring that none of the observed absorptions is assignable to the MoO molecule. The three vibrational frequencies assigned to $(MoO_3)_2$ were observed to shift from 975.7, 694.2, and 350.1 $cm^{-1}$ for $^{16}O$ to 934.8, 660.4, and 332.7 $cm^{-1}$ for $^{18}O$ in Ne matrices, yielding $\nu^{18}/\nu^{16}$ ratios of 0.9581, 0.9513, and 0.9503, respectively.

For the $MoO_2$ molecule, it is possible to calculate the O-Mo-O bond angle, 2α, from the observed, symmetrically substituted isotopic frequencies. The formulas which are commonly employed in this type of calculation are only rigorously correct for molecules conforming to potential energy functions which are strictly quadratic in their dependence on the atomic displacements. However, the values for bond angles which are obtained by using the observed fundamentals in the calculations are usually found to be good approximations to the actual values, and the calculations reported here must be viewed with recognition of the approximation inherent in them.

For a non-linear $XY_2$ molecule having a Y-X-Y bond angle of 2α the asymmetric stretching frequencies for the normal molecule ($\omega_3$) and the symmetrically substituted molecule ($\omega_3^i$) are related to the isotopic masses and the bond angle, 2α,

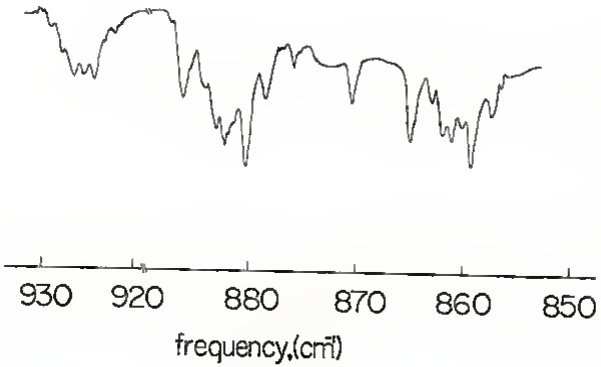


Figure 38. High resolution infrared absorption spectrum of a Ne matrix containing Mo oxides formed at high temperatures (21°C) using $^{18}O_2$.

by the following relation [33]:

$$\left(\frac{\omega_3^i}{\omega_3}\right)^2 = \frac{m_X m_Y (m_X^i + 2m_Y^i \sin^2\alpha)}{m_X^i m_Y^i (m_X + 2m_Y \sin^2\alpha)} ,$$

where the superscript (i) has been used to designate quantities referring to the isotopic molecule. Solving this equation for $\sin\alpha$ yields

$$\sin\alpha = \left[\frac{m_X m_X^i [\omega_3^2 m_Y - (\omega_3^i)^2 m_Y^i]}{2m_Y m_Y^i [(\omega_3^i)^2 m_X^i - \omega_3^2 m_X]}\right]^{1/2} .$$

By substituting into this equation the atomic weights and observed frequencies for the isotopic modifications of $MoO_2$, the bond angle, 2α, was found to be 124° ± 6°. This bent configuration accounts for the presence of the absorption assigned to $\nu_1$, the symmetric stretch, and its weak intensity relative to the $\nu_3$ vibration.

Photolysis of Mo and $O_2$ in a Ne matrix.--As an attempt to produce the MoO molecule by a technique other than high temperature reaction of the metal with $O_2$ gas, an experiment was performed in which Mo atoms were vapor deposited in a Ne matrix doped with 0.1 percent $O_2$ by volume. After the deposit the matrix was examined for absorption features in the infrared region from 4000-200 $cm^{-1}$ and in the near infrared, visible, and ultraviolet regions from 1200-240 nm. The matrix showed no absorption features other than those attributable to Mo atoms, which have been discussed previously. The matrix was then subjected to the radiation from a flowing $H_2$ electrodeless discharge through a LiF window for about 1 hour

and reexamined spectroscopically. No new features were noted in the near infrared, visible, or ultraviolet regions, but the strong Mo atom absorptions which were present before the photolysis were completely destroyed by exposure to the $H_2$ lamp radiation. In the infrared, however, several new absorption bands appeared below 2000 $cm^{-1}$. Figure 39 shows the new features which were observed. The strong band near 1040 $cm^{-1}$ was examined under higher resolution to determine the nature of the fine structure seen in Figure 39. Figure 40 is the resulting expansion of the 1040 $cm^{-1}$ peak, which was resolved into 4 absorptions at 1042.6, 1039.7, 1038.1, and 1036.9 $cm^{-1}$. It is obvious that the observed fine structure does not correspond to the previously discussed Mo isotopic pattern.

The most intense absorption of the 1040 $cm^{-1}$ system occurs at 1039.7 $cm^{-1}$ and appears to be assignable to the $\nu_3$ frequency of the $O_3$ molecule. This vibration is seen in the gas phase at 1042.1 $cm^{-1}$ [34]. Brewer and Wang have reported this vibration to occur at 1035 $cm^{-1}$ in Kr matrices and as a doublet between 1025 and 1030 $cm^{-1}$ in Xe matrices [35]. Andrews and Spiker have observed the ozone molecule in Ar matrices at 16°K where they found the $\nu_3$ vibration to occur at 1039.6 $cm^{-1}$ with a shoulder at 1033.5 $cm^{-1}$ [36]. The absorption at 702.1 $cm^{-1}$ corresponds to the $\nu_2$ vibration which appears at 701.0 $cm^{-1}$ in the gas phase [37], and at 704.5, 700, and 695 $cm^{-1}$ in Ar, Kr, and Xe, respectively [35,36]. The weak $\nu_1$ vibration which is expected near 1100 $cm^{-1}$ was not observed in this experiment.

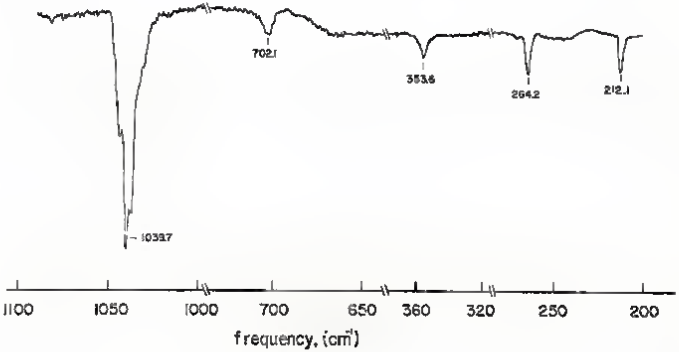


Figure 39. Infrared absorption seen after $H_2$ photolysis of a 0.1% $O_2$ in Ne matrix containing Mo atoms.

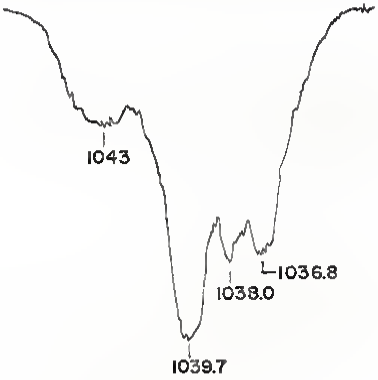


Figure 40. High resolution scan of the 1040 $cm^{-1}$ band shown in Figure 39.

The absence of the Mo atom absorption bands after the photolysis and the new infrared absorptions at 353.6, 264.2, and 212.1 $cm^{-1}$ which appeared after the photolysis suggest the presence of other molecules in the matrix in addition to $O_2$ and $O_3$. The work of Andrews et al. on the matrix reactions of $O_2$ with metal atoms suggests that these features may be due to the isterionic vibrations of species of the form $M^+O_2^-$ or $MO_2M$ [38]. These vibrations have been reported for the Cs-$O_2$ system [38], and the strongest absorptions were found to occur at 357, 269, and 236 $cm^{-1}$ in Ar matrices. Of course to definitely assign these vibrations for the Mo-$O_2$ system $^{18}O$ substitution would be necessary for each molecule.

## Discussion

A most remarkable observation is the extreme difference of the electronic spectra of the Mo oxides when compared with the W oxides [2]. In the W-$O_2$ experiments [2] which were quite similar to the Mo-$O_2$ experiments reported here, the WO molecule was readily isolated and observed to exhibit seven electronic transitions between 350 and 600 nm, whereas in the Mo-$O_2$ system there was no evidence to suggest that any MoO was ever formed. The dioxide, $MoO_2$, was isolated and observed along with the trioxide, $MoO_3$, and other polymeric Mo oxides in the infrared spectra, but no electronic progressions were found that could be specifically assigned to any of these species. $WO_2$, on the other hand, was shown to exhibit an extended electronic progression between 600 and 800 nm in Ar

and Ne matrices.

Previous discussions have pointed out that one might expect to find similarities between second and third row transition metal oxides of the same group [39,40]. However, considerable differences among the oxides of a given group have been found and explained on the basis of the variation of the electronic configurations of the metal atoms in a group. For example, Zr and Hf atoms both have $d^2s^2$ ($^3F$) electron configurations and their monoxides both have $^1\Sigma^+$ ground states [39,40]. In the group VB metals, Nb and Ta, the NbO molecule was found to have a $^4\Sigma^-$ ground state in contrast to the $^2\Delta_r$ ground state of TaO [3]. The Nb atom has a $d^4s$ ($^6D_{1/2}$) electron configuration, whereas the Ta atom possesses a $d^3s^2$ ($^4F_{3/2}$) ground state [24]. A similar situation arises for the group VIB metals, where Cr and Mo have $d^5s$ ($^7S_3$) ground states in contrast to W, where the intrusion of the f shell makes the $d^4s^2$ configuration more stable and the ground term is $^5D_0$ [24]. This apparently results in a bonding schema for W oxides which is quite different from the Mo oxides as has been seen from their electronic spectra. This suggests that the ground state of MoO is like that of CrO rather than WO. The ground state of CrO is thought to be $^5\Pi$ [41-43] while that of WO is probably $^3\Sigma^-$ [2].

The infrared spectra of the oxides of Mo produced by vaporizing $MoO_3$(s) and passing $O_2$ gas over the hot metal have been observed in Ne and Ar matrices at 4°K. By comparing the spectra obtained under different experimental conditions, one can attempt to assign bands to individual molecules as

has been done in the preceding sections. Table 14 contains a summary of the most intense features which were observed in Ne matrices and the molecules to which they were assigned.

A comparison of the infrared spectra of the Mo oxides with the reported vibrational frequencies for the corresponding W oxides [2] in Table 15 indicates that the Mo oxides are more weakly bonded than those of tungsten. If for $MoO_2$ a valence force field is assumed, one may calculate the force constant, $k_1$, for the Mo=O bond from [44]

$$\lambda_3 = 4\pi^2\nu_3^2 = (1 + \frac{2m_0}{m_{Mo}} \sin^2\alpha) \frac{k_1}{m_0} ,$$

where $m_0$ and $m_{Mo}$ are the masses of oxygen and Mo, and $\alpha = 62°$ is 1/2 the O-Mo-O bond angle of 124° which was calculated above. This gives a value for $k_1$ of $6.3 \times 10^5$ dyne/cm which is considerably smaller than the value of $9.6 \times 10^5$ dynes/cm obtained for the W system.

The polymeric oxides of the two metals seem to be more similar. The trioxides both have the planar ring configuration shown in Figure 32, and recent infrared observations of the vapor over $WO_3$(s) have shown a spectrum having peaks at 810 and 960 $cm^{-1}$ [45]. This compares extremely well with the spectrum of the vapors over $MoO_3$(s) which exhibits absorption peaks at 815 and 969 $cm^{-1}$ [9]. Both of these gas phase systems consist primarily of the trimers and tetramers, and therefore it appears that the matrix vibrational spectra of these molecules should be very similar. This suggests that the frequencies assigned to $(WO_3)_3$ (1024, 874, and 487 $cm^{-1}$) [2]

TABLE 14

VIBRATIONAL FREQUENCIES OF MOLYBDENUM OXIDE MOLECULES FROM INFRARED SPECTRA OF NEON MATRICES

| Molecule | $\nu(^{16}O)\,cm^{-1}$ | $\nu(^{18}O)\,cm^{-1}$ | $(\nu^{18}/\nu^{16})$ |
|---|---|---|---|
| $MoO_2$[a] | 900.1 | 859.3 | 0.9546 |
| | 949.5 | 896.8 | 0.944 |
| $MoO_3$[a] | 976.7 | 933.3 | 0.9556 |
| | 922.2 | 880.3 | 0.9546 |
| $(MoO_3)_2$ | 975.7 | 934.8 | 0.9581 |
| | 694.2 | 660.4 | 0.9513 |
| | 350.1 | 332.7 | 0.9503 |
| $(MoO_3)_3$ | 977.6 | | |
| | 858.4 | | |
| | 840.1 | | |
| $(MoO_3)_4$ or $(MoO_3)_5$ | ∿973 | | |
| | 896.2 | | |
| | 884.0 | | |
| | 865.9 | | |
| | 514.1 | | |

[a]For bands in which the Mo isotope structure was resolved, the listed frequency corresponds to the most abundant isotope, $^{98}Mo$.

TABLE 15

COMPARISON OF W AND Mo OXIDES IN NEON MATRICES AT 4°K

| Molecule | Vibration | Vibrational Frequency ($cm^{-1}$) | |
|---|---|---|---|
| | | Mo Oxides | W Oxides |
| $MO_2$ | $\nu_1$ | 949.5 | 992 |
| | $\nu_3$ | 900.1[a] | 928 |
| $MO_3$ | | 976.7[a] | 1040 |
| | | 922.2[a] | 1007 |
| $(MO_3)_3$ | | 977.6 | 1024 |
| | | 858.4 | 874 |
| | | 840.1 | |
| | | | 487 |

[a]For bands in which the Mo isotope structure was resolved, the listed frequency corresponds to the most abundant isotope, $^{98}Mo$.

should be reexamined with careful attention being given to the 950-970 $cm^{-1}$ region since from the $(MoO_3)_3$ results one would expect the highest frequency absorption to occur there rather than above 1000 $cm^{-1}$.

## REFERENCES, CHAPTER III


1. E.A. Gulbraneen, Corrosion 26(1), 19 (1970).

2. W. Weltner, Jr. and Donald McLeod, Jr., J. Mol. Spectry. 17, 276 (1965).

3. J. Brom, Jr., C.H. Durham, Jr., and W. Weltner, Jr., accepted for publication by Journal of Chemical Physics.

4. W. Weltner, Jr. and Donald McLeod, Jr., J. Chem. Phys. 42, 882 (1965).

5. G. Piccardi, Atti. Acad. Nazl. Lincei 17, 654 (1933).

6. T.M. Swaminathan and S.G. Krishnamurthy, Current Sci. (India) 23, 258 (1954).

7. A. Gatterer, S.J., J. Junkas, S.J., and E.W. Salpeter, S.J., Molecular Spectra of Metallic Oxides (Specola Vaticana, Vatican City, Italy, 1957).

8. J.C. Howard and J.G. Conway, J. Chem. Phys. 43, 3055 (1965).

9. T.V. Iorns and F.E. Stafford, J. Am. Chem. Soc. 88, 4819 (1966).

10. V.S. Nikitin and A.A. Mal'tsev, Vestn. Mosk. Univ. Khim. 24(5), 109 (1969).

11. P.A. Perov, V.N. Novikov, and A.A. Mal'tsev, Vestn. Mosk. Univ. Khim. 27(1), 89 (1972).

12. W. Krassar, Naturwissenschaften 1969, 213 (1969).

13. G. Anderson and A. Magneli, Acta Chem. Scand. 4, 793 (1950).

14. F. Schoch and E. Kay, J. Chem. Phys. 59, 718 (1973).

15. D. Green and D.M. Gruen, J. Chem. Phys. 60, 1797 (1974).

16. J. Barkowitz, M.G. Inghram, and W.A. Chupka, J. Chem. Phys. 26, 842 (1957).

17. R.P. Burns, G. DeMaria, J. Drowart, and R.T. Grimsley, J. Chem. Phys. 32, 1363 (1960).

18. J.B. Berkowitz-Mattuck, A. Buchler, J.L. Engelke, and S.T. Goldstein, J. Chem. Phys. 39, 2722 (1963).

19. J. Drowart, G DeMaria, R.P. Burns, and M.G. Inghram, J. Chem. Phys. 32, 1366 (1960).

20. G. DeMaria, R.P. Burns, J. Drowart, and M.G. Inghram, J. Chem. Phys. 32, 1373 (1960).

21. W. Weltner, Jr., P.N. Walsh and C.L. Angell, J. Chem. Phys. 40, 1299 (1964).

22. A.G. Worthing, Phys. Rev. 25, 853 (1925).

23. W. Espe, Materials of High Vacuum Technology, vol. 1 (Pergamon Press, Oxford, 1966), p. 88.

24. C.E. Moore, Atomic Energy Levels, NBS Circular 467, vol. 2 (1952).

25. G.W. Robinson, J. Mol. Spectry. 6, 58 (1961).

26. L. Brewer, B. Meyer and G.D. Brabson, J. Chem. Phys. 43, 3973 (1965).

27. J.H. Ammeter and D.C. Schloenagle, J. Chem. Phys. 59, 4784 (1973).

28. M. Erith and O. Schnepp, J. Chem. Phys. 39, 2714 (1963).

29. W. Weyhmann and F.M. Pipkin, Phys. Rev. 137(2), A 490 (1965).

30. M. McCarty, Jr., J. Chem. Phys. 52, 4973 (1970).

31. E.Z. Zasorin, N.G. Rambidi and P.A. Akishin, Acta Crystallogr. 16, A130 (1963).

32. R.L. Heath in Handbook of Chemistry and Physics, 48th edition, R.C. Weast, Ed., (The Chemical Rubber Co., Cleveland, Ohio, 1967) p. B-29.

33. G. Herzberg, Infrared and Raman Spectra of Polyatomic Molecules, (D. Van Nostrand Company, Inc., New York, 1945)p. 228.

34. S.A. Clough and F.X. Kneizys, J. Chem. Phys. 44, 1855 (1966).

35. L. Brewer and J.L.F. Wang, J. Chem. Phys. 56, 759 (1972).

36. L. Andrews and R.C. Spiker, Jr., J. Chem. Phys. 59, 1863 (1973).

37. D.J. McCaa and J.H. Shaw, J. Mol. Spectry. 25, 374 (1968).

38. L. Andrews, J.T. Hwang, and C. Trindle, J. Phys. Chem. 77, 1065 (1973).

39. W. Waltner, Jr. and D. McLaod, Jr., J. Phys. Chem. 69, 3488 (1965).

40. W. Waltner, Jr., Science 155, 155 (1967)

41. W.F.C. Ferguson, J. Res. Nat. Bur. Std. 8, 381 (1932).

42. C. Ghosh, Z. Physik 78, 521 (1932).

43. M. Ninomiya, J. Phys. Soc. Japan 10, 829 (1955).

44. G. Herzberg, Infrared and Raman Spectra of Polyatomic Molecules, (D. Van Nostrand Company, Inc., New York, 1945) p. 169.

45. V.I. Yampol'skii and A.A. Mal'tsev, Russ. J. Inorg. Chem. 15 (7), 1029 (1970).

## BIOGRAPHICAL SKETCH

Warren Dewey Hewett, Jr. was born July 4, 1948, at Palatka, Florida. He is the son of Warren D. Hewett and Evelyn June Hewett. He was graduated from Palatka Senior High School in Palatka, Florida in June 1966. He attended St. Johns River Junior College and the Florida State University, receiving his Bachelor of Science degree in Chemistry in June, 1969. He worked as a graduate research assistant in the Department of Chemistry at the University of Florida from August, 1969, until August, 1974. He is married to the former Mary Theresa Kynard. They have one child, Amy Elizabeth.

I certify that I have read this study and that in my opinion it conforms to acceptable standards of scholarly presentation and is fully adequate, in scope and quality, as a dissertation for the degree of Doctor of Philosophy.

W. Weltner, Jr., Chairman
Professor of Chemistry

I certify that I have read this study and that in my opinion it conforms to acceptable standards of scholarly presentation and is fully adequate, in scope and quality, as a dissertation for the degree of Doctor of Philosophy

W. E. Ferson
Professor of Chemistry

I certify that I have read this study and that in my opinion it conforms to acceptable standards of scholarly presentation and is fully adequate, in scope and quality, as a dissertation for the degree of Doctor of Philosophy.

W. R. Dolbier, Jr.
Associate Professor of Chemistry

I certify that I have read this study and that in my opinion it conforms to acceptable standards of scholarly presentation and is fully adequate, in scope and quality, as a dissertation for the degree of Doctor of Philosophy

S. O. Colgate
Associate Professor of Chemistry

I certify that I have read this study and that in my opinion it conforms to acceptable standards of scholarly presentation and is fully adequate, in scope and quality, as a dissertation for the degree of Doctor of Philosophy.

R. W. Fahien
Professor of Chemical Engineering

This dissertation was submitted to the Graduate Faculty of the Department of Chemistry in the College of Arts and Sciences and to the Graduate Council, and was accepted as partial fulfillment of the requirements for the degree of Doctor of Philosophy.

August, 1974

Dean, Graduate School